
Combining Hydroacoustics Data with Landsat Images to Map Seagrass Cover and to Identify Spatial Pattern Predictors (Historically Low Rainfall, Benthic Topography and Hurricanes) of Long-Term Change (1984 to 2021) in a Jamaican Marine Protected Area

[Kurt McLaren](#)^{*}, Jasmine Sedman^{*}, [Karen McIntyre](#)^{*}, Kurt Prospere^{*}

Posted Date: 26 February 2024

doi: 10.20944/preprints202402.1414.v1

Keywords: climate change; storms; submerged aquatic vegetation; random forest



Preprints.org is a free multidiscipline platform providing preprint service that is dedicated to making early versions of research outputs permanently available and citable. Preprints posted at Preprints.org appear in Web of Science, Crossref, Google Scholar, Scilit, Europe PMC.

Copyright: This is an open access article distributed under the Creative Commons Attribution License which permits unrestricted use, distribution, and reproduction in any medium, provided the original work is properly cited.

Article

Combining Hydroacoustics Data with Landsat Images to Map Seagrass Cover and to Identify Spatial Pattern Predictors (Historically Low Rainfall, Benthic Topography and Hurricanes) of Long-Term Change (1984 to 2021) in a Jamaican Marine Protected Area

Kurt McLaren ^{1,*}, Jasmine Sedman ¹, Karen McIntyre ² and Kurt Prospere ³

¹ Department of Geography and Environmental Sciences, Northumbria University, Ellison Place, Newcastle upon Tyne NE1 8ST, UK

² CL Environmental Co. Ltd., Kingston 10, Jamaica; karenenvironment@yahoo.com

³ kprospere@caribbeanbiodiversityfund.org

* Correspondence: kurt.mclaren@northumbria.ac.uk

Abstract: Despite increased protection globally, climate change and other anthropogenic factors have caused a significant decline in seagrass cover. Identifying the specific causes of this decline is paramount if they are to be addressed. Therefore, we identified the causes of long-term change in seagrass/submerged aquatic vegetation (SAV) percentage cover and extent in the Bluefields Bay Special Fish Conservation Area (BBSFCA), a marine protected area on Jamaica's southwestern coast. We used two random forest regression (RFR) models that included 2013 hydroacoustic survey SAV percentage cover data (dependent variable), and auxiliary data, reflectance data from level 2 processed 2013 Landsat 7 and 8 images and image band texture statistics maps (mean and variance) as predictors to generate 24 SAV percentage cover maps for the period 1984 – 2021 (37 years) using data from Landsat 4-5, 7 and 8 images., from which benthic features maps (SAV present, absent and coral reef) were created. Rainfall and map data were used to determine if SAV extent/area (km²) and average percentage cover and annual rainfall changed significantly over time and to evaluate the influence of rainfall. Rainfall impact on the overall spatial patterns of SAV loss, gain, and percentage cover change was assessed using a pixel-based regression. Finally, the most important spatial pattern predictors (two rainfall proxies (distance and direction from river mouth), benthic topography, depth, and hurricane exposure (a measure of hurricane disturbance)) of SAV loss, gain, and percentage cover change during 23 successive 1-to-4-year periods were identified using spatial Bayesian INLA generalized linear mixed models. SAV area/extent was largely stable with > 70% mean percentage cover for multiple years. However, Hurricane Ivan (in 2004) caused a significant decline in SAV area/extent (by 1.62 km², or a 13%) during 2002 – 2006 and a second hurricane (Dean) in 2007 delayed recovery until 2015. Additionally, rainfall declined significantly by >1000 mm since 1901, and mean monthly rainfall positively influenced SAV percentage cover change. The pixel-based regression highlighted areas where mean monthly rainfall had a positive overall effect on SAV cover percentage change (across the entire bay) and gain (closer to the mouth of a river). The most frequently selected important spatial pattern predictors were the two rainfall proxies (areas closer to the river mouth were more likely to experience SAV loss and gain) and depth, with shallow areas generally having a higher probability of SAV loss and gain. Three hurricanes had significant but different impacts depending on their distance from the southern coastline. Hurricane Gilbert, which made landfall in 1988, resulted in higher SAV percentage cover loss in 1987 - 1988. Benthic locations with a northwestern/northern facing aspect (the predominant direction of Ivan's leading edge wind bands) experienced higher SAV losses during 2002 – 2006. Although some locations impacted by Ivan and not by Dean recovered during 2006 – 2008, exposure to Ivan explained percentage cover loss during 2006 – 2008 and average exposure to (the cumulative impact of) Ivan and Dean (both with tracks close to the southern coastline) explained SAV loss during 2010 – 2013. Therefore, despite historic lows in annual rainfall, overall, higher rainfall was beneficial, multiple hurricanes impacted the site, and despite two hurricanes in three years SAV recovered within a decade. Hurricanes and a further reduction in rainfall may pose a serious threat to SAV persistence in the future.

Keywords: climate change; storms; submerged aquatic vegetation; random forest

1. Introduction

Seagrasses are a group of flowering plants that can exist fully submersed in a marine environment [1,2]. However, seagrasses are largely found in shallow areas with clear waters due to their dependence on light for photosynthesis and because there is greater light attenuation with increased depth and turbidity [3]. They provide key ecological services including sediment stabilization, organic carbon production and distribution, nutrient cycling, and many other services in the marine environment [1]. They are one of the most productive ecosystems in the world as they provide shelter and food to communities of animals [2,4,5]. When compared with adjacent bare substrata, a larger number and a greater diversity of fish are generally found in dense sea grass beds [4,6]. Seagrass meadows are therefore an important nursery habitat for many commercially important fish species [5]; as a result, they are vital for commercial fisheries as they support the productivity of 20% of the biggest fisheries in the world [2,5]

Seagrasses are however, being significantly impacted by anthropogenic activities in coastal zones and by climate change [1,2,7]. As a result, globally, seagrass extent/area is largely declining [8]. There is therefore a need to implement effective conservation and management strategies to stymie the loss of these important marine ecosystems and to restore their functionality [2,9]. One commonly used/implemented strategy is the establishment of Marine Protected Areas (MPAs). But establishing marine protected areas alone may not be sufficient as some of the threats to seagrasses are terrestrial in origin [2]. Addressing these threats will require integrated land-sea or ridge-to-reef conservation planning [10–12], but this is seldom incorporated in MPA management/conservation efforts [10]. Moreover, the frequency of high intensity storms [1,13,14], the duration, frequency, and intensity of droughts [15] and rainfall variability [16] have increased due to climate change. As a result, in some tropical areas, and in the Caribbean in particular, tropical storms, cyclones/hurricanes [17–21], droughts [19,21] and extreme rainfall events [22] are increasingly becoming important threats to the persistence of seagrass beds, as they can result in increased stress, catastrophic losses/die off and degradation despite added protection.

Effective management and conservation of seagrasses affected by climate change and anthropogenic disturbances is contingent on the availability of baseline data on their cover, distribution, and dynamics [20] and the impact of threats. These data can be used to inform or guide conservation/management strategies, but they are rarely available [7]. Also, there is a need for improved spatial assessments of seagrasses, and this should be complemented by a more extensive assessment of seagrass health and threats, so that management or conservation actions can be implemented to reverse their impacts [2]. Remote sensing, particularly optical remote sensing, can provide frequent data on seagrass distribution over a wide range of temporal and spatial scales. Maps generated from optical remote sensors are often used to assess and document changes due to natural hazards (e.g. [17,20]) and anthropogenic activities (e.g. [23,24]). These maps can be used to inform management, conservation and planning decisions or actions pertaining to the implementation of a management plan [25]. However, optical remote sensors are primarily used to produce categorical/thematic maps, which are essentially binary measures/indicators of seagrass presence/absence [26]. Percent cover is generally considered to be a better measurement parameter than presence/absence [26], as it is a good, accurate, sensitive, and responsive measure or indicator of spatial and temporal changes in seagrass condition and abundance [21]. Additionally, quantifying the continuous heterogeneity in seagrass cover will enhance our capacity to describe real landscapes and increase our understanding of seagrass spatial dynamics [26].

Generating maps of percentage cover from optical sensor data will require extra data and/or analysis (e.g. [27–29]) or alternatively, active remote sensors, such as single or multibeam sonars (SBES or MBES) can be used [26,30,31]. The increased availability of active remote sensors, particularly SBES, have increased our ability to acquire and/or generate spatially explicit datasets of

seagrass percentage cover (and height) and benthic topography cost effectively [30]. In addition, hydroacoustic percentage cover data can be combined with passive remote sensor data to produce maps of seagrass percentage cover (e.g. [31]). Moreover, GIS data layers of the spatial extent and/or the magnitude of threats or possible predictors of seagrass change can also be obtained and inputted into statistical spatial or spatio-temporal regression models together with other predictors (benthic topography) and maps of seagrass dynamic change (loss, gain, or percentage cover change) and used to identify spatial pattern predictors or predictors of spatial change (e.g. [24]). Spatial pattern predictors or spatial pattern causes/drivers are one of several groups of factors that are generally used within the land use and landcover change (LULC) framework to explain the cause or drivers of change [32]. These factors generally represent the biophysical characteristics of a landscape that are neither the root cause nor direct human actions that leads to land change, but instead they determine where changes will occur [32,33]. If applied to seagrass changes within a marine environment, they can be used to represent biophysical factors (e.g. benthic topography, climate, extreme weather/climatic events (sensu [33]) that are similarly neither the root cause nor direct human actions that can determine where changes will occur on the benthos. This will help to increase our understanding of the patterns and causes of changes and can be used to inform reasonable and specific planning for sustainable management [34].

In this study, we used a method outlined in [31] to build random forest models that combined a 2013 seagrass percentage cover hydroacoustic dataset from the Bluefields Bay Special Fish Conservation Area (BBSFCA), a marine protected area (MPA) found on the southwestern coast of Jamaica, with 2013 Landsat 7 and 8 reflectance data and other auxiliary data for the site. These models were then applied to Landsat 4-5, 7 and 8 images collected over the period 1984 – 2021 to predict seagrass percentage cover, from which binary presence/absence maps were generated. We used these maps or data from these maps with rainfall data from the site, benthic topography maps (depth, slope, aspect, and benthic position index), GIS layers of proxies to rainfall and a measure of hurricane severity/impact to identify the most important landscape and spatial pattern predictors of seagrass loss, gain, and percentage cover change over the 37-year period. Despite being protected, the site was impacted by past hurricanes, and there is evidence that a river that drains into the bay might also be impacting seagrass cover [30]. Therefore, it is important to determine how these factors influence seagrass cover change.

2. Materials and Methods

2.1. Study Site

The study area is the Bluefields Bay Special Fish Conservation Area (BBSFCA) (18°10'02" N, 78°02'02" W). It is a Marine Protected Area (MPA) that was established on July 28, 2009, and it is found on the southwest coast of Jamaica in the parish of Westmoreland, in south-western Jamaica (Figure 1a,b). It is 13.82km² in size [30] and a large percentage of the shoreline/ intertidal zone comprises mangrove stands (41.7%), followed by sandy beach (35.5%) and the remaining shoreline consists of naturally occurring limestone bedrock and cliffs or manmade structures including rip rap, sea walls, and boulder/ rubble (22.8%) [35]. The predominant benthic features in the bay include seagrass beds dominated by *Thalassia testudinum* and a smaller area dominated by *Halodule wrightii*, unconsolidated bare sediment with sparse algal cover, including *Halimeda* sp., unconsolidated bare sediment, and coral reef (McIntyre et al. 2018). There were three hurricanes that may have affected Bluefields Bay during the study period. These included Hurricanes Gilbert (1988), Ivan (2004) and Dean (2007). Hurricane Gilbert made landfall on September 12, 1988, and had an average windspeed of 204 – 213 km hr⁻¹. Hurricanes Ivan and Dean passed at a distance of 40.3 km and 40.9 km, respectively, from the eyes of the two hurricanes to the closest point along the southern coastline of Jamaica on September 11, 2004, and August 20, 2007, respectively, and had an average windspeed of 241 – 250 km hr⁻¹ and 231 km hr⁻¹, respectively [36] (Figure A4).

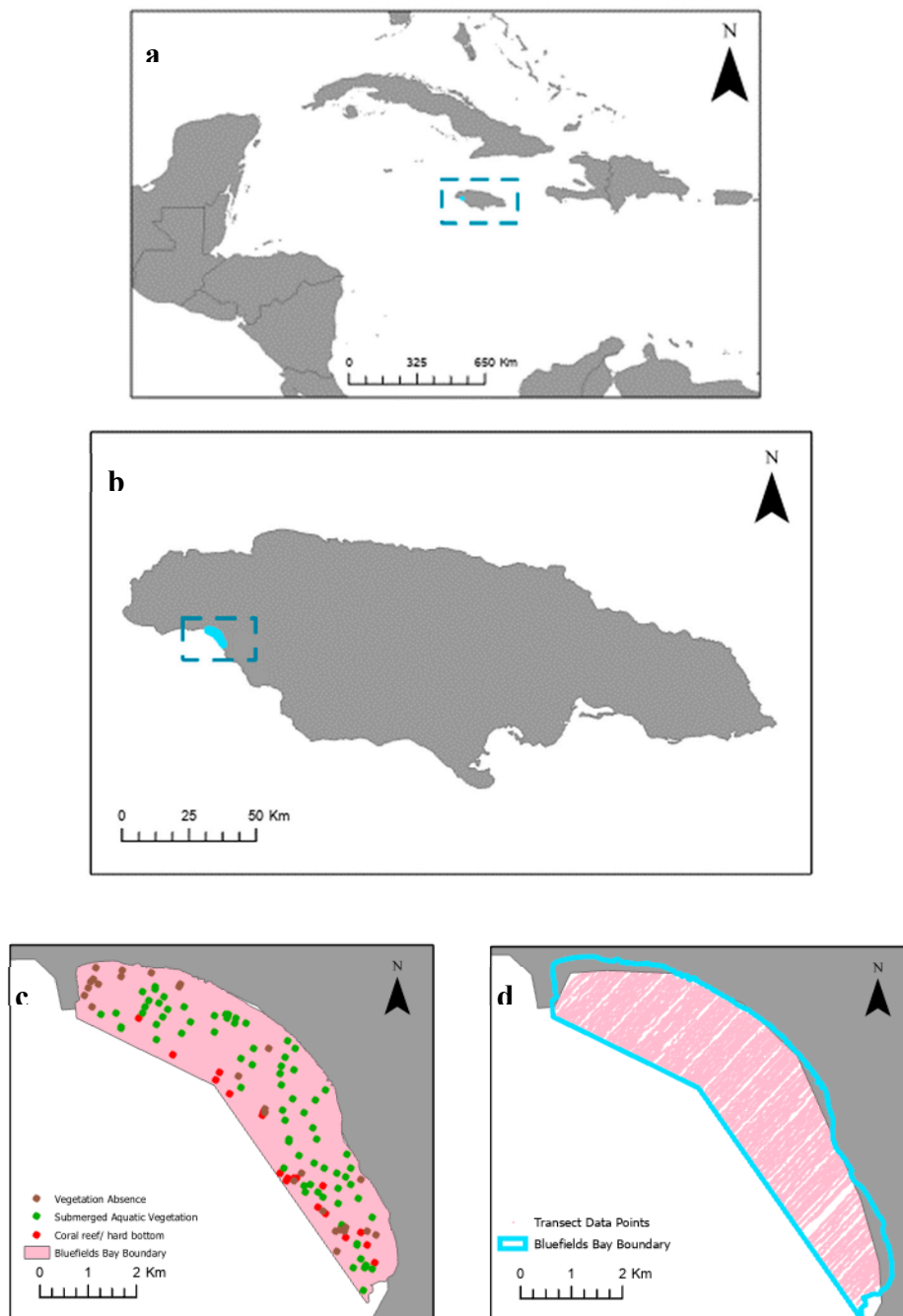


Figure 1. Maps showing a) the Caribbean region, b) the location of the Bluefields Bay Special Fish Conservation Area (BBSFCA) on the southwestern coast of Jamaica, c) location of reference samples used for accuracy assessments and d) the hydroacoustic survey tracks.

2.2. Satellite Imagery

In total, 27 satellite images of the study site from 1984 to 2021 (37 years) were downloaded from the United States Geological Survey (USGS) website (<https://earthexplorer.usgs.gov/>) (Table A1). We only chose images with no turbidity. Also, we tried as much as possible to include images that were collected during same time of the year corresponding to the first (January – Mid-April) or the second dry season (July to August) to ensure consistency, but several images used were collected during the major rainy season (Sept. – Dec). Nevertheless, comparisons between and among images from different years can be improved if the atmospheric conditions at the time when the images were captured are accounted for or removed. As such, Landsat Collection 2 Level 2 images, which is an atmospherically corrected surface reflectance image product, were downloaded and used. The image

bands were stacked and reprojected to the local datum, JAD 2001. The 2006 and 2013 Landsat 7 images had missing data (SLC off) and therefore, the mosaic function in ArcGIS Pro (2.5.1) was used to merge two 2006 and 2013 images that were collected three and five months apart (see Table A1), respectively, to fill in the gap of this missing data.

2.3. *Hydroacoustic auxiliary data*

Processed hydroacoustic survey data from [30,35] were used in this study. The hydroacoustic survey was conducted during the period July 26 – 2 August 2013 and the data were collected using a 206 kHz Biosonics DT-X split-beam side mounted transducer [30]. The transducer had a beam width of 7°, which approximated to a footprint size of 0.01 to 0.05 m² at a depth of 1–2m [30] and it was multiplexed to allow for simultaneous sampling of macrophytes (0.4 m/s pulse duration) and other benthic features [30]. During the survey, horizontal positioning data (± 0.30 m) were obtained from a Starfix HP Differential GPS and the survey was conducted along predefined transect tracks with 50 m spacings, covering 294.178 km [30] (Figure 1d). The hydroacoustic data were processed using two software packages: VBTTM (Biosonics Inc.), which was used to derive depth values that were spatially referenced and were subsequently corrected for tidal differences and reprojected to the local datum and EcoSAV™ (Biosonics Inc.), which was used to derive percentage seagrass or submerged aquatic vegetation (SAV) cover data that were also spatially referenced [30].

The spatially referenced, reprojected, and tide corrected depth data points were interpolated using universal kriging to create a bathymetric surface model [30], from which a bathymetric position index (BPI) and a rugosity map was created. The BPI map was created after applying the “Land Facet Corridor Designer Tools” for ArcGIS 10 [37] to the BSM layer [31]. The BPI map data have continuous values that change from negative to positive; this represents a transition from valleys to slopes and then to ridge tops. “Block Statistics” was used to create the rugosity map in ArcGIS 10.6 [31]. Grey Level Co-Occurrence Matrix (GLCM) maps were generated in the R programming language environment [38,39] using the “glcm” package [40]. The package was used to calculate texture statistics (mean and variance) derived from grey-level co-occurrence matrices (GLCMs) for bands 1, 2 and 3 for Landsat 4-5 and 7 images, and bands 1, 2, 3 and 4 for Landsat 8 images. Specifically, average GLCM textures in all directions were calculated using shifts of 45 degrees for the image bands and these were outputted as maps of mean and variance GLCM textural measures.

2.4. *Random Forest models and model validation*

SAV percentage cover maps were produced from integrating the spatially referenced SAV data with Landsat image reflectance data and auxiliary data using random forest regression (RFR) models following [31]. Before the SAV maps were produced, the SAV data were split into training (78% or 107,076 data points) and validation (12% or 14,853 data points) data. The validation data were selected using a random start and every tenth data point transects, and transects perpendicular to the shoreline [30]. Additionally, before the RFR models were built, the coordinates of the track points where SAV percentage cover data were generated, were used to extract data from maps of the auxiliary data (BSM [depth] and BPI) and band reflectance and GLCM mean and variance data from the images for the year 2013 (bands 1 – 3 for the composite Landsat 7 image with the missing data filled in and bands 1 – 4 for Landsat 8 image). Images from the year 2013 were used because the hydroacoustic survey was conducted during this time. Two RFR models were built using the “randomForest” package [41] in R, both of which included SAV percentage cover data at each track point as the dependent variable and BSM and BPI as predictors. One of the two models included the extracted 2013 composite Landsat 7 bands reflectance and GLCM data as additional predictors and the other RFR model included the 2013 Landsat 8 bands reflectance and GLCM data as additional predictors. After each model was built and run, the predicted SAV cover at each validation data point was generated by the models. These were then compared to the observed SAV cover at each validation data point and the following validation criteria were generated: mean absolute percentage error (MAPE), root mean squared error (RMSE), mean absolute error (MAE), mean squared error (MSE), bias (a measure of consistent under- or over-forecasting; BIAS), relative bias (rBIAS), and

relative mean separation (rMSEP). See [42] for the formulations. Small values of MSE, RMSE, MAE, rBIAS and rMSEP (lower values or values close to zero) imply that the model is suitable for making predictions, robust and that predicted values are very similar to observed values. Also, for the MAPE, values close to 0 represent the most accurate predictions, however all values of MAPE below 100% represent accurate predictions.

Following validation, the most accurate model was then chosen. For the Landsat 8 model, this included all the predictors, whereas for the Landsat 7 model this included the top 5 predictors (Figure A1; Table A2). A polygon shapefile of the BBSFCA was converted to a 2 m gridded raster, and then to a points shapefile. These data points were used to extract data from the auxiliary maps and reflectance and GLCM mean and variance maps for the Landsat 4-5, 7 (1984 – 2010) and 8 (2015 – 2021) images and for the 2013 images used for modelling. The RFr model for each Landsat series was then used to predict SAV cover at each point of the point grid for each year of a particular Landsat series using the predictors extracted for each point. For example, the Landsat 7 RFr model was used to predict SAV cover using reflectance data from Landsat 4 – 5 and 7 images plus the auxiliary data. Similarly, the Landsat 8 RFr model was used to predict SAV cover using reflectance data from Landsat 8 images plus the auxiliary data. No Landsat 4- 5 images could be found close to the year of the hydroacoustic assessment (the closest was 2011). Moreover, the wavelength intervals/bandwidth for the Landsat 7 bands were the same as the Landsat 4- 5 bands; therefore, the Landsat 7 RFr model was used to predict SAV coverage using Landsat 4 – 5 image data. The predictions were exported as a 2m gridded raster, and a single SAV percentage cover map was produced for each year (24 maps in total).

2.5. Benthic habitat maps and accuracy assessments

Several binary maps for each of the percentage cover maps generated using the 2013 Landsat 7 and 8 series image data were created using different threshold values in raster calculator in ArcGIS Pro 3.0.1. The thresholds used were 23%, 25%, 28%, 30%, 35%, 38% and 40% for the 2013 Landsat 7 and 8 derived SAV percentage cover maps. The range of values used was previously found to generate the most accurate binary maps [31]. The binary maps created were added to a coral reef map that was generated using a threshold of 0.23 for the rugosity map, also in raster calculator (following [31]). From this, maps with three classes, SAV present, SAV absent and coral reef, were produced for the maps derived from the two datasets. A total of 118 accuracy assessment (AA) reference data points (21, 23 and 74, coral reef, vegetation absent and present points, respectively), collected by [30] in 2013 at randomly determined points using georeferenced videos/video camera drops (Figure 1), were used to identify the most accurate threshold for each map. The map classes at each AA location were first determined by using the AA points to extract information from the maps on the classes found at each location. An accuracy assessment was then conducted in R using the “asbio” package [43] using the extracted classes and reference data for each map. The most accurate threshold with the highest overall agreement (OA) was identified (following [31]) for the two series (Figure A3). However, we chose the threshold with the second highest OA for the Landsat 4-5 and 7 maps and used it to generate a benthic habitat map for each year during the period 1984 – 2010 (30% SAV cover threshold) and we used the second of two thresholds with the highest OA for the Landsat 8 maps to create maps for the period 2013 – 2021 (25% SAV cover threshold). These thresholds were chosen because they consistently produced maps that closely matched (visually) the unclassified images.

2.6. Assessment of landscape scale change and predictors of change in SAV cover and area over time

Mean SAV percentage cover and SAV total area for each year for the entire bay was determined and were used to assess changes overtime and the possible effects of rainfall on SAV percentage cover and area. Additionally, monthly rainfall data for the site (Bluefields Bay) for the period 1901 to 1994 were obtained from the Jamaican Meteorological Service. This dataset did not cover the entire period of this study and as such, this was supplemented using monthly rainfall data from Savanna-la-Mar, the capital of the parish of Westmoreland, which is located ≈ 5.6 km away. A generalized additive mixed model (GAMM) with an autoregressive moving average (ARMA) error structure (used to

account for temporal autocorrelation) and a cubic smoothing spline was used to determine if there was a significant trend in total annual rainfall over time. For this assessment, only years that included data for all months were used. A GAMM was also used to determine if there were significant changes/trends in SAV percentage over and SAV total area over the period 1984 – 2021. The GAMM was implemented using the “mgcv” package [44–47]. The ARMA error structure was defined by two parameters: the number of autoregressive (AR) (p), and the number of moving average (MA) parameters (q) [48]. The autoarima function from the “forecast” package [49,50] was first used to determine the most suitable number of ARMA parameters based on AIC, AICc (AIC corrected for finite sample sizes) and BIC (Bayesian information criterion) values. It was applied to the residuals from a generalized additive model (GAM) that included the dependent and independent variables with no ARMA error structure. The ARMA values obtained from the GAM using autoarima function were used in the GAMM. Before final models were accepted, the autocorrelation and partial autocorrelation functions (ACF and PACF, respectively) were used to check the residuals (normalized for the GAMM) of the models to determine if they were white noise (random and not autocorrelated). Additionally, the model parameters (GAMM) and the 95% confidence intervals of the AR, MA were checked to ensure that they did not include zero. This indicated that there were no problems with the error structure and the model contained an adequate number of explanatory variables. A generalized linear regression (GLM) with a gaussian link function, implemented using the “lme4” package [51], was used to determine if there was a relationship between monthly SAV percentage cover and area change, and average monthly rainfall. Monthly values were determined using the number of months between the dates when two consecutive Landsat images were recorded. For example, for the 1984 (09/10/1984) and 1985 (02/03/1985) images, the number of months between the two dates was determined (4.8), and the total rainfall, the change in percentage SAV cover and the change in total area of SAV between the two dates were divided by the number of months. This was repeated for the other image dates. The R-squared values for the GLMs were generated using the “MuMIn” package [51].

2.7. The spatial pattern predictors of SAV change

Pixel-based regressions were used to assess the effects of rainfall on the spatial pattern of SAV loss and gain and changes in percentage cover over the period 1984 - 2021. First, maps of binary (1 for loss or gain and 0 for no change) and percentage cover change were generated by subtracting one image year from the subsequent year. A total of 23 maps for each category of assessment, that is, binary loss, gain, and percentage cover change, were therefore produced. A logistic GLM implemented using the “lme4” package with a quasibinomial distribution (to account for under or over dispersion) and a logit link function was then used to model the relationship between the binary map values (1 or 0) at each pixel and total monthly rainfall. The relationship between the percentage cover change per month map values (change divided the time (months) between consecutive maps) at each pixel and rainfall was modelled using a linear regression. The outputs from the regressions, particularly the marginal (for the logistic GLM) or adjusted (for the linear regression) R-squared, gradient estimate and P value at each pixel, were represented as maps. These maps highlighted locations on the ground that were directly influenced by rainfall positively or negatively over the study period.

We then assessed the influence of proxies to rainfall, that is proximity/Euclidian distance and cardinal direction from the mouth of the main river that empties into the bay, and other possible predictors such as topographic features including aspect and slope, and depth and exposure to past hurricanes or exposure vulnerability (EV) (Figure A3), on the spatial patterns of SAV loss, gain and percent cover change between successive time periods (i.e., 1984 – 1985, 1985 – 1986, etc.). EV is a unitless measure that has been previously used to link the heterogeneity of hurricane exposure to responses shown by terrestrial vegetation at sites that experienced hurricane disturbance [52]. Although EV maps have primarily been used and validated in a terrestrial context, they were used in this study to determine if they can also explain changes in SAV cover and extent due to damage caused by/changes induced by hurricanes (to seagrass beds) in a nearshore marine environment. For

this assessment, EV maps were generated following the method outline in [36,52]. A DEM and information on windspeed and direction as the hurricane passed by Jamaica or made landfall are needed to create EV maps. The BSM of the bay was used in place of a DEM and information on windspeed and direction was obtained from actual and proxy images of the three hurricanes. These were available as processed ultra-high resolution QuikSCAT Scatterometer images of Hurricane Ivan and Dean (available at: <http://www.scp.byu.edu/data/Quikscat/HRstorms.html>) and were obtained as a .gif file and rectified to the Jamaican datum, JAD 2001. The images included the circular hurricane wind bands color-coded according to wind speed (in knots) that were overlaid with wind flags (wind direction) (Figure A4). Images of Ivan at its closest point to and after it passed Jamaica were available, but there were no images of Hurricane Ivan before, Dean before and Dean as it passed by Jamaica, and there were no images of Hurricane Gilbert, because the QuikSCAT images are only available for the period 1999–2009. As such, images of Ivan and Dean after they passed Jamaica, and a proxy processed ultra-high resolution QuikSCAT image that closely matched a satellite image of Hurricane Gilbert (Hurricane Ivan (September 11, 2004)) as it passed over Jamaica were used [36,52] (Figure A4).

Before the EV maps were generated, tracks of three hurricanes were downloaded as an ESRI point shapefile file from the National Oceanic and Atmospheric Administration (NOAA), NOAA's International Best Track Archive for Climate Stewardship (IBTrACS) website (<https://www.ncei.noaa.gov/products/international-best-track-archive>) [53,54] and re-projected to the Jamaican datum, JAD 2001. The imagery 'Georeference' function in ArcGIS Pro was used to center the image of Hurricane Dean and the proxy image of Gilbert on track point locations, which represented the approximate location of the hurricane's eye before they passed, at their closest point to and after they went passed Jamaica. The two images of Hurricane Ivan did not need to be centered, but an image of the hurricane after it passed Jamaica was centered on a point corresponding to the proximate location of the eye before it passed Jamaica (Figure A4). At each location, wind flags found close to Bluefields Bay were digitized as polylines in ArcGIS Pro and the 'Linear Directional Mean' function was used to determine wind direction from the polylines. Windspeed was estimated from the colour coded wind bands by using the upper range or value for wind speeds ≥ 35 knots (64 km hr^{-1}). There were no wind speed values > 50 knots (93 km hr^{-1}), which were generally found closer to the track points. Windspeed was therefore estimated by averaging windspeed at the track point where the image was centered (this information was available in the attribute table of the tracks) and 93 km hr^{-1} . Maps of topographic exposure for various wind directions were generated using the 'hillshade' function/feature in ArcGIS Pro with the BSM (following [55,56]). Wind direction was used as the azimuth angle and a fixed wind inflection angle of 20° was used (following [52]) in the 'hillshade' function. Hillshade maps of exposure for each location and for each hurricane were generated and used in the following formula in the raster calculator in ArcGIS Pro:

$$EV = (\sum_{i=1}^n (\text{wind speed}_i * \text{hillshade map of exposure}_i)) / n, \quad (1)$$

where i is one of several locations where the actual or proxy hurricane image(s) was (were) located or centered and evaluated (e.g., location (i) = 1, 2, 3, 4...) and n is the total number of locations evaluated/hillshade maps created. A single EV map of each hurricane was generated (Figure A3), and additionally, the EV maps for Ivan and Dean were averaged. Average EV of multiple hurricanes can also be an important predictor of vegetation response over time when two or more hurricanes impacted a site [36,52].

The SAV loss, gain and percent cover change maps were converted to point shapefiles, appended with the X and Y coordinates at each point, and used to extract values of the predictors at each point. The relationship between SAV loss, gain and percent cover change and the predictors at each point for successive years was then evaluated. These datasets were large and spatially autocorrelated, and there are very few methods that can efficiently handle such datasets. As such, we used a Bayesian approach based on the Integrated Nested Laplace Approximation (INLA), implemented using the 'INLA' package [57–61] due to its flexibility and ability to efficiently handle large spatial data [59,62]. We developed Hierarchical Bayesian models with a spatial random effect that were formulated according to a spatially explicit generalized linear mixed model (GLMM)

framework. Therefore, the response variable at each successive period or overall and plot location was assumed to follow a distribution from an exponential family. Consequently, appropriate distributions and link functions were chosen for the response variables such as a zero-inflated binomial Type 1 (ZIB.1) or a binomial (if the model failed to converge) distribution with a logit link function for the binary loss and gain data and a Gaussian distribution for the percentage change data. The chosen exponential family parameters (θ) were linked to a structured additive predictor η by their link function $g(\cdot)$, so that $g(\theta) = \eta$ and the linear predictor was defined as:

$$\eta = \beta_0 + \beta_1 * a + \beta_2 * b + f(s), \quad (2)$$

where η was the linear predictor for the response variables, β_0 was the intercept and β_1 and β_2 were the (linear) regression coefficients for the predictors a and b . The random effect (spatial) was introduced using the semiparametric function $f(\cdot)$ [59]. The $f(s)$ represented a spatially-structured (s) random effect. The spatial location of each transect point (the X, Y coordinates) was used as the basis of the spatial random effect. The Stochastic Partial Differential Equation (SPDE) approach of [58] was used to model the spatially structured random effect as a Gaussian random field (GRF). The SPDE method subdivides the domain or the area of interest into non-intersecting triangles, creating an index mesh instead of a regular grid [58]. Linear combinations of basis functions, defined on the locations of the set of vertices, are used in triangulation process [58]. Please see [58] for a more detailed explanation of the SPDE approach. In this study the area of the MPA was used as the domain to approximate the spatial fields. To reduce boundary effects (where the variance is twice as large as inside the domain), the mesh did not extend beyond the study area.

The default and recommended priors, that is vague priors or estimations of non-informative priors [63], were used to develop the models. Additionally, the penalized complexity prior (PC-prior) framework of [64] was adopted to remove or avoid overfitting particularly for the spatially structured effect, which was found to be operating at a smaller (but neither at a similar nor higher) spatial scale than the covariates or predictors of the models [65]. When this occurred, the spatial effect explained the data better than the covariates and the model was meaningless [65]. Additionally, model accuracy and the marginal R-squared were inflated while the Deviance Information Criterion (DIC) was deflated, and as a result, they could not be used for model selection. To correct this, a weakly informative PC-prior derived by [64] was used to define the model parameters for the SPDE model as the practical range and the marginal standard deviation. The PC-prior penalised complexity by shrinking the range to infinity and the marginal variance to zero [64]. Several values for the range were used (starting with half the distance between the furthest points), until there was no overfitting.

Before the statistical tests were performed, the Spearman's rho statistic and test were used to identify significantly correlated independent variables (with a correlation of > 0.55). Additionally, a Deviance Information Criterion (DIC) that is computed in R-INLA, which is analogous to the Akaike Information Criterion (AIC) but it is more suitable for hierarchical Bayesian models [66] was generated for each model. This was used to compare the goodness-of-fit of the models; specifically, models with the lowest DIC values were generally considered as the best. The marginal R-squared (following [67]) was also used to assess model fit. It was calculated as follows:

$$100 * (1 - (\sum_{t=1}^t \sum_{n=1}^n (depend - fitted)^2 / \sum_{t=1}^t \sum_{n=1}^n (depend - \text{mean}(depend))^2)), \quad (3)$$

where t is time when n subjects were considered, *depend* is the response variable, and *fitted* are the values predicted by the model. Model validation was conducted using a k (five) fold cross-validation using the validation criteria used previously for the Rfr models. A receiver operating characteristic (ROC) curve value (AUC) was calculated for the SAV loss and gain models using the "pROC" package [68] in R and used as an additional measure of model accuracy.

We scaled all our models so that they had a generalized variance equal to 1 and to ensure that the precision parameters for different covariates or intrinsic models were comparable or had the same interpretation [69]. In general, it is usually difficult to identifying the 'best' parsimonious model because competing models can often describe the same data just as well (Whittingham et al., 2006). We therefore applied stringent model selection criteria, but we prioritized the use of the validation criteria, and model selection included several steps. We first determined the most suitable type of

regression, that is, either a linear or polynomial (and the order of the polynomial) regression, for modelling the relationship between each predictor and the dependent variable. All the orders a polynomial regression must be important (the Bayesian equivalent to a significant frequentist relationship) before it was accepted if it was found to be more suitable (based on the DIC and marginal R-squared values). The linear form of the predictor was used during model selection if the relationship (linear or polynomial) between the predictor and the dependent variable was not important. All possible combinations of predictors were then evaluated, and we used the DIC and marginal R-squared values to choose the best 2 to 8 models. For the chosen models, all predictors had to be important and uncorrelated (with a correlation coefficient of ≤ 0.55 and they were not linearly or monotonically correlated). A 5-fold cross-validation was then used to validate the best models and the AUC was calculated for each model. The final parsimonious model, which yielded the most accurate predictions and had uncorrelated predictors for at each successive period, was then selected. The final models included the most important predictors for each period, but they may not have the lowest DIC and the highest marginal R-squared and AUC, as again, model accuracy was prioritized for model selection. In addition to reporting the best model, we reported the top 2 to 8 most accurate parsimonious models and their accuracies (Tables S1-3).

3. Results

The RFr models used to generate SAV percentage cover maps from the Landsat 4-5 and 7 and the Landsat 8 satellite series data explained 62.7% and 69.8% of the variance in the data and were reasonably accurate with a MAE of 19.2% and 17.7%, respectively, a very low or marginal bias and a RMSE of 25.6% and 24.4%, respectively (Table A2.). Importantly, the MAPE was less than 100% indicating that the models were ideal for predicting (Table A2). The most important predictor was BPI followed by reflectance data for bands 1 and 4 for the Landsat 4-5 and 7 and Landsat 8 series models, respectively (Figure A1). The chosen thresholds had an OA of 78% and 75% for the Landsat 7 and Landsat 8 three class maps, respectively (Figure A2). It was assumed that the binary maps for all the other years will likely have similar accuracies (it would be difficult to assess past accuracies without in-situ reference data for each year). The percentage cover and binary maps with coral reef class added in (benthic features map) are presented in Figures 2 and 3. Percentage cover varied across the bay over time, with an area close the mouth of the river consistently having the lowest SAV percentage cover and this area was largely classified as SAV absent in the benthic features maps, when the thresholds were applied (Figures 2 and 3). For the years 1990, 1999, 2000, 2013, 2015 and 2019, most of the bay ($> 70\%$) had a percentage cover of $> 80\%$ (Figure 2). For 1993, most of the bay had a percentage cover of $\leq 60\%$, but generally, for all other years there was a higher SAV percentage cover found across the bay (up to 80%) (Figure 2). A notable shift in the pattern of SAV presence/absence occurred in 2006, with the area of the SAV absent class around the mouth of the river increasing and this class was found extensively across the south of the bay for the first time (Figure 3). This change was attributed to the impact of Hurricane Ivan in 2004.

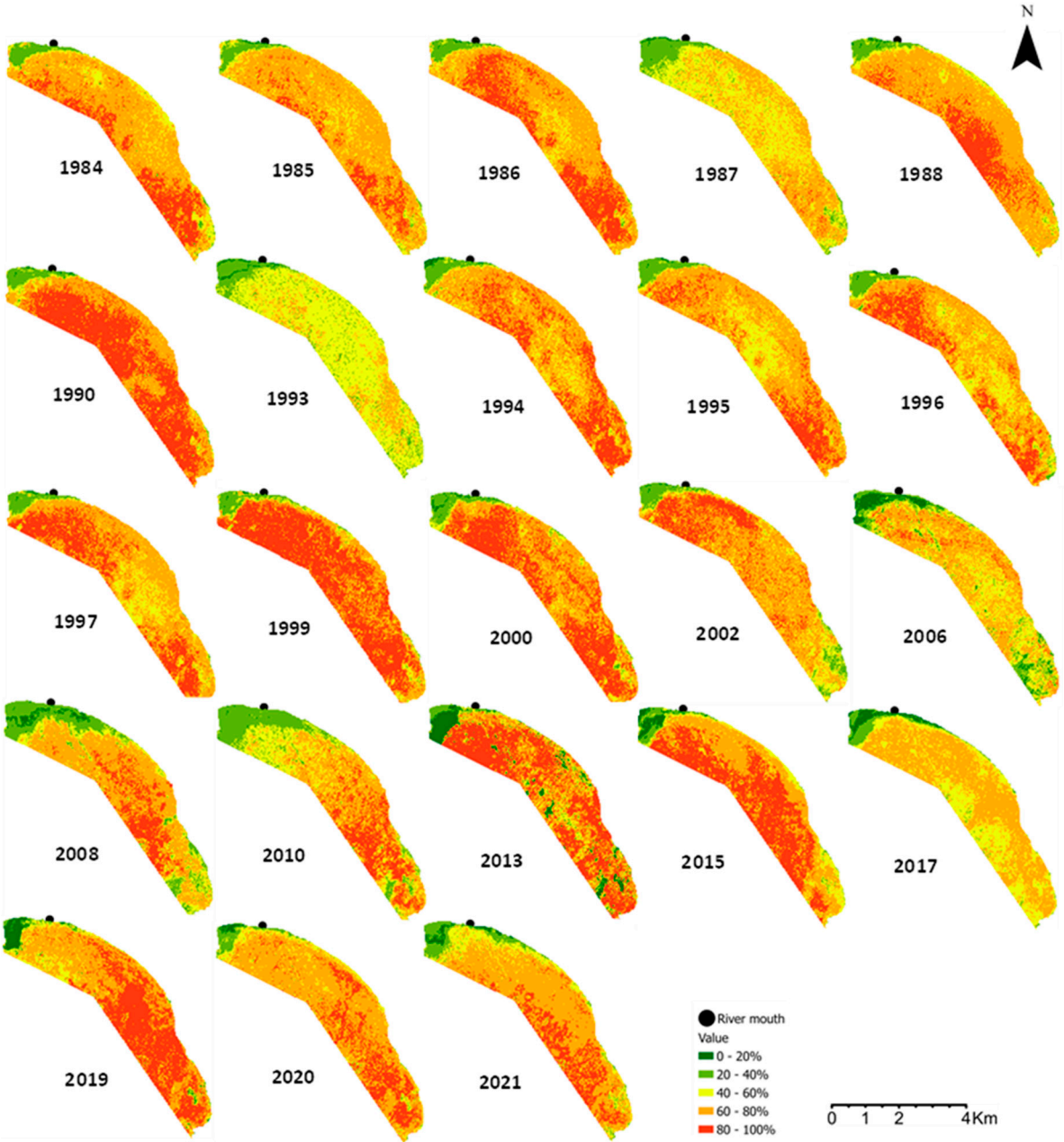


Figure 2. Maps of submerged aquatic vegetation percentage cover in the Bluefields Bay Special Fish Conservation Area (BBSFCA), Westmoreland, Jamaica that were produced/predicted by Landsat 7 and 8 random forest regression models for the period 1984 – 2021.

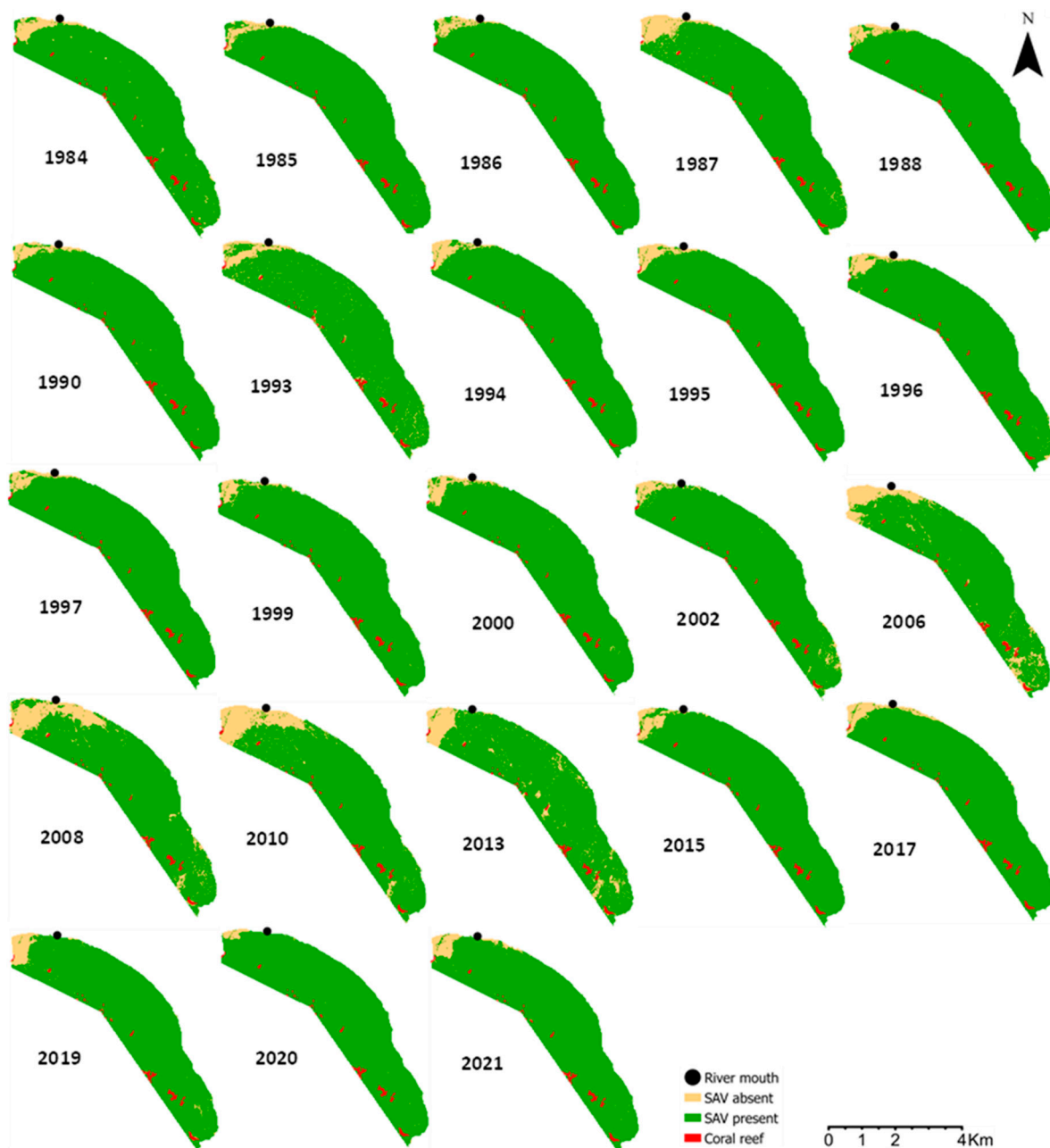


Figure 3. Maps of benthic features in the Bluefields Bay Special Fish Conservation Area (BBSFCA), Westmoreland, Jamaica for the period 1984 – 2021 that were produced by applying a threshold to submerged aquatic vegetation (SAV) percentage cover maps generated from the SAV random forest regressions.

3.1. Landscape scale changes and predictors

The total area of SAV changed significantly over time (Table 1), with a significant reduction in SAV occurring in 2006 (Figures 3 and 4a), which was the largest recorded decline. Recorded loss for the period was 1.62 km², or a 13% decline at a rate of -0.04 km² month⁻¹. Recovery after 2006 was not complete until 2015 (Figures 3 and 4a). The change in extent between 2002 - 2006 coincided with the year when Hurricane Ivan passed by the island (2004) and during the subsequent period (2006 – 2008), Hurricane Dean passed close by the island (Figures A4). The extent of SAV loss in 2006 occurred over a larger area (Figures 2 and 3), but in general, SAV change (loss and gain) mainly occurred close to the river as this was an area of active change (Figure 3). Average percentage cover for the entire bay did not change significantly over time and there were 11 years with an average of > 70% percentage cover with the lowest being 49.8% in 1993. Percentage cover change over successive

years was influenced by rainfall (Figure 4b; Table 1), with higher positive percentage cover change occurring when rainfall was higher. Despite the importance of higher rainfall, annual rainfall at the site during the study period was significantly lower than at the start of the 20th century (approximately 1000 mm lower on average), as there was a significant decrease in annual rainfall (Figure 4c; Table 1).

Table 1. Results obtained from a generalized additive model (GAM), a generalized additive mixed model (GAMM) with an autoregressive moving average (ARMA) error structure and a generalized linear model (GLM) used to assess the trend in total (annual) rainfall over time (1901 – 2021), the trend in total area of submerged aquatic vegetation (SAV) over the study period (1984 – 2021) and the relationship between monthly SAV percentage (perc.) cover change and rainfall over the study period, respectively, for Bluefields Bay, Jamaica.

Models and correlation structure	Parameter	Value	L 95% CI	U 95% CI	S.E.	t/F	P	Adj. R ² / R ²
Rainfall (mm) x Year (GAM)	Intercept	1943.6			42.4	45.9	<0.001	34.7%
	s(Year)					50.5†	<0.001	
SAV total area (km ²) x Year (GAMM) ARMA (2, 0)	Intercept	11.9			0.02	686.5	<0.001	69.5%
	s(Year)					71.7†	<0.001	
	Phi 1	-0.76	- 1.25	- 0.26				
	Phi 2	-0.43	- 0.77	0.02				
SAV perc. cover change (month ⁻¹) x Rainfall (mm month ⁻¹) (GLM)	Intercept	-1.28			0.43	-2.95	0.0077	28.9%
	Rainfall	0.012			0.004	2.99	0.007	

L, U and CI = lower and upper confidence intervals; SE = standard error; adj R² = adjusted R²; Phi = autoregressive coefficient; s() = cubic smoothing spline; t = t distribution; F and † = F distribution.

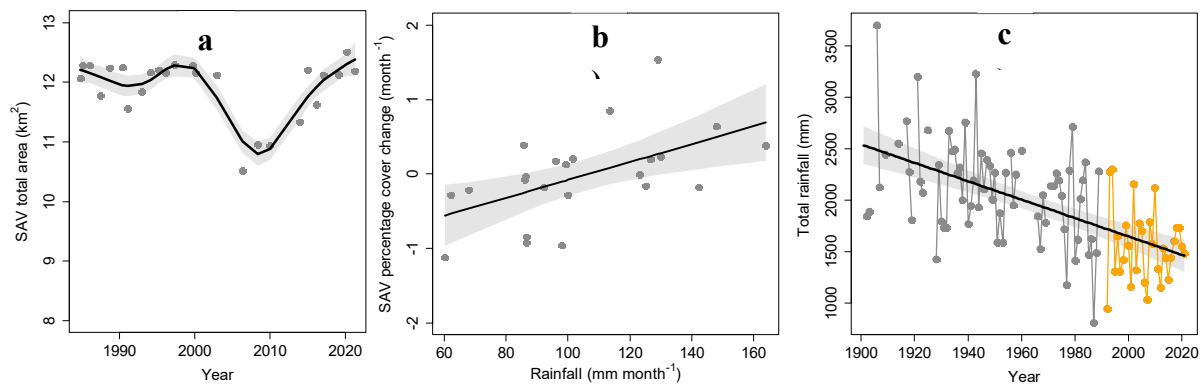


Figure 4. Observed and predicted values obtained from our analyses using a) a generalized additive mixed model (GAMM) with an autoregressive moving average (ARMA) error structure to assess change in total area of SAV over time in the Bluefields Bay Special Fish Conservation Area (BBSFCA), Westmoreland, Jamaica, b) a generalized linear regression (GLM) with a gaussian link function used to determine the influence of monthly rainfall on SAV percentage cover change in the BBSFCA, and c) a generalized additive model (GAM) used to assess the changes in total annual rainfall from 1901 to 2021 over time for Savanna-la-mar, the capital of Westmoreland, and the BBSFCA. Shade = standard error.

3.1. Spatial pattern predictors

The pixel-based regression was used to determine if rainfall influenced the spatial patterns of SAV loss, gain, and percentage area change. For loss and gain, this was found to be confined largely to a small area, which was close to the mouth of the main river towards the northwestern section of the bay (Figure 5). The influence of rainfall on both loss and gain was negative and positive, that is, SAV probability of loss or gain increased or decreased with an increase in monthly rainfall (Figure 6). There were more locations with a probability of SAV loss declining or the SAV gain increasing as rainfall increased than areas with the opposite trend (Figure 5). Rainfall influenced SAV percentage cover change over a larger area of the bay (when compared with SAV loss and gain), and these were interspersed with areas that were not affected (Figure 5). Also, rainfall had both a positive and negative effect on percentage cover change with the predominant effect being positive (Figures 5 and 6).

We identified the most important spatial pattern predictors of SAV cover loss, gain, and percentage cover change to determine other possible influences on change. All final models that included the most important predictors had an AUC of > 0.6 . Marginal R-squared values for important predictors of SAV loss ranged from 0.2% – 19.2%, with the highest value being obtained during the 2008 – 2010 period (Figure 7). The third (2002 – 2006) highest R-squared value (15.5%; Figure 7) was obtained during the period when SAV loss was highest after the passage of a single hurricane in 2004. A single predictor of SAV loss was found to be important during 13 of the 23 periods assessed whereas multiple predictors were important for the remaining periods (Figure 8). Like the pixel-based regression results, the important predictors had a positive or a negative effect on SAV loss (Figures 8 and 12a–c), and the relationship between SAV loss and the predictors were either linear (SAV loss increased or decreased with an increase in BSM, aspect, slope, distance, direction, or EV) or they were better explained by a polynomial regression (Figures 8 and 12a–c) indicating that their effects varied across a range of predictor values. The most frequent important predictors of SAV loss were direction (11 intervals) and distance (7 intervals) from the mouth of the river, followed by aspect, BSM, slope and then average EV (6, 6, 2 and 1 intervals, respectively) (Figure 8). This highlighted the importance of rainfall (which influences river outflow), as the probability of SAV loss declined significantly as distance from the river mouth increased (e.g. Figure 12c) for 6 of 7 intervals it was important (the parameter estimates were (largely) negative (Figure 8)). Moreover, nearly all the relationships with direction from river (10 of 11), were positive, indicating

that the highest probability of loss occurred largely to the southwest to northwest of the river mouth (Figure A3). Only during the 2002 – 2006 period the probability of loss was higher to the east of the river mouth as well as the southwest to the northwest (Figure 12b). Additionally, SAV loss was more likely to occur in shallow areas (4 of the 6 intervals), that is, there was a positive relationship with BSM. BSM values are negative (Figure A3); therefore, a positive relationship indicates a greater probability of loss in shallow areas (Figure 8). The results also highlighted the possible impact of two hurricanes. Aspect was an important predictor of the probability of loss during the period when Ivan passed by the island (2002 – 2006). Aspect is used in the calculation of EV and is a proxy to the predominant direction of exposure to hurricane winds [36,52]. Our results show that SAV loss was greatest at benthic locations with a northwestern and a northern facing aspect (Figure 12g,h) and this corresponded with the prevailing wind direction of the leading edge of the outer wind bands of Ivan (Figure A4). Also, during this period, the probability of loss for the first time was higher to the east and southwest – northwest of the river mouth (therefore loss occurred in more than one direction) (Figures 12b and A3). Furthermore, average EV (for Ivan and Dean) was an important predictor during the 2010 – 2013 period, where SAV loss was positively associated with higher average EV (Figures 8 and 12a).

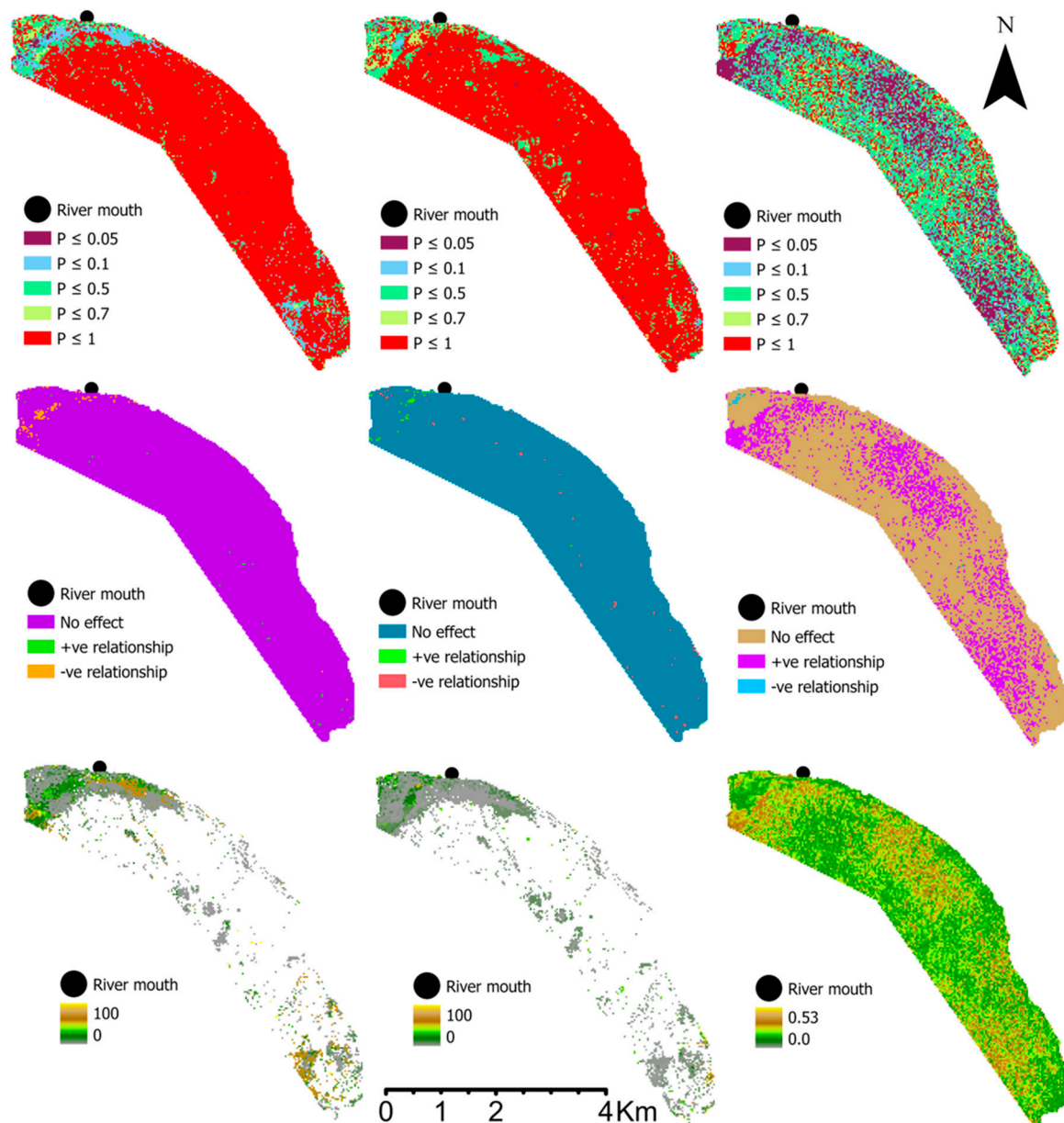


Figure 5. Results obtained from the pixel-based regression used to assess the influence of monthly rainfall on the spatial pattern of SAV loss (left column, top to bottom), gain (middle column, top to bottom) and percentage cover change (right column, top to bottom) in the Bluefields Bay Special Fish Conservation Area (BBSFCA), Westmoreland, Jamaica. The outputs from the regressions are presented as maps and include the p-value (top row), the sign (+ or -) of the regression slope (middle row) and the R^2 values.

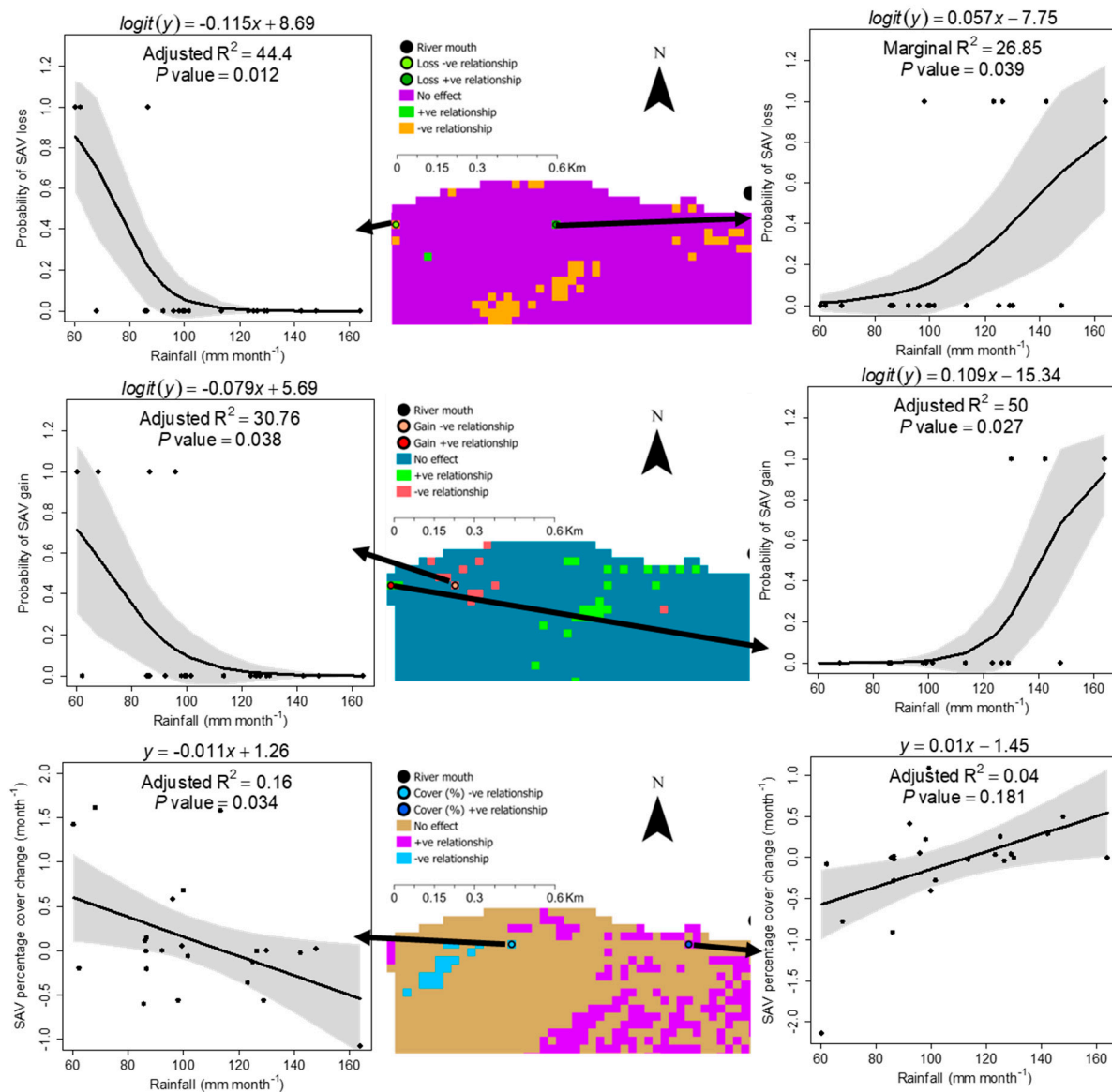


Figure 6. Examples of observed and predicted values for negative (in left column) and positive (in the right column) relationships identified by the pixel-based regressions that were used to assess the influence of monthly rainfall on the spatial pattern of SAV loss (top row), gain (middle row) and percentage cover change (bottom row) in the Bluefields Bay Special Fish Conservation Area (BBSFCA), Westmoreland, Jamaica. Dashed blue lines = standard error.

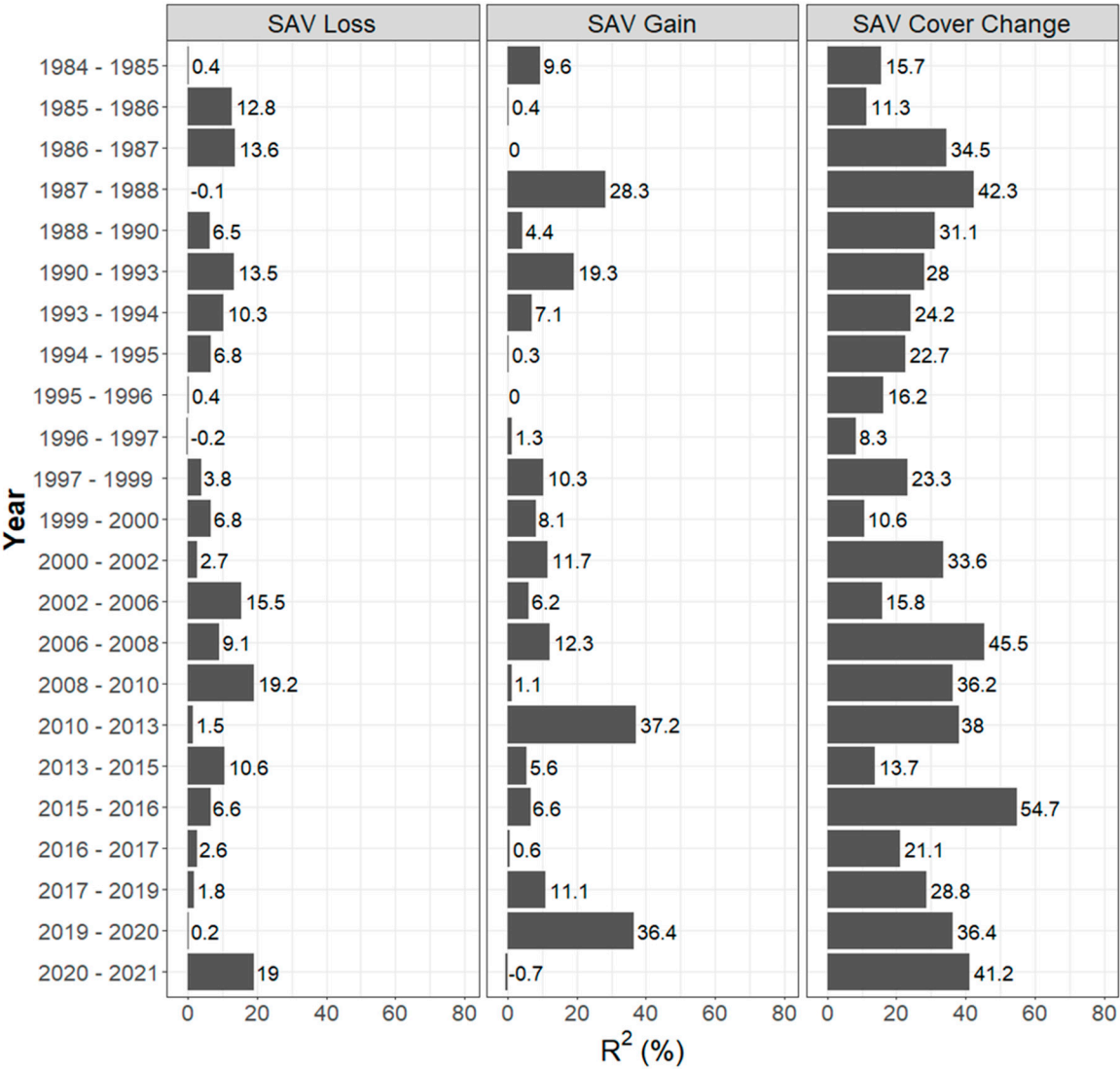


Figure 7. Marginal R-squared values calculated for the final parsimonious Bayesian Integrated Nested Laplace Approximation (INLA) models that included the most important spatial pattern predictors of SAV loss, gain, and percentage cover change in the Bluefields Bay Special Fish Conservation Area (BBSFCA), Westmoreland, Jamaica for 23 successive 2-to-4-year periods between 1984 – 2021.

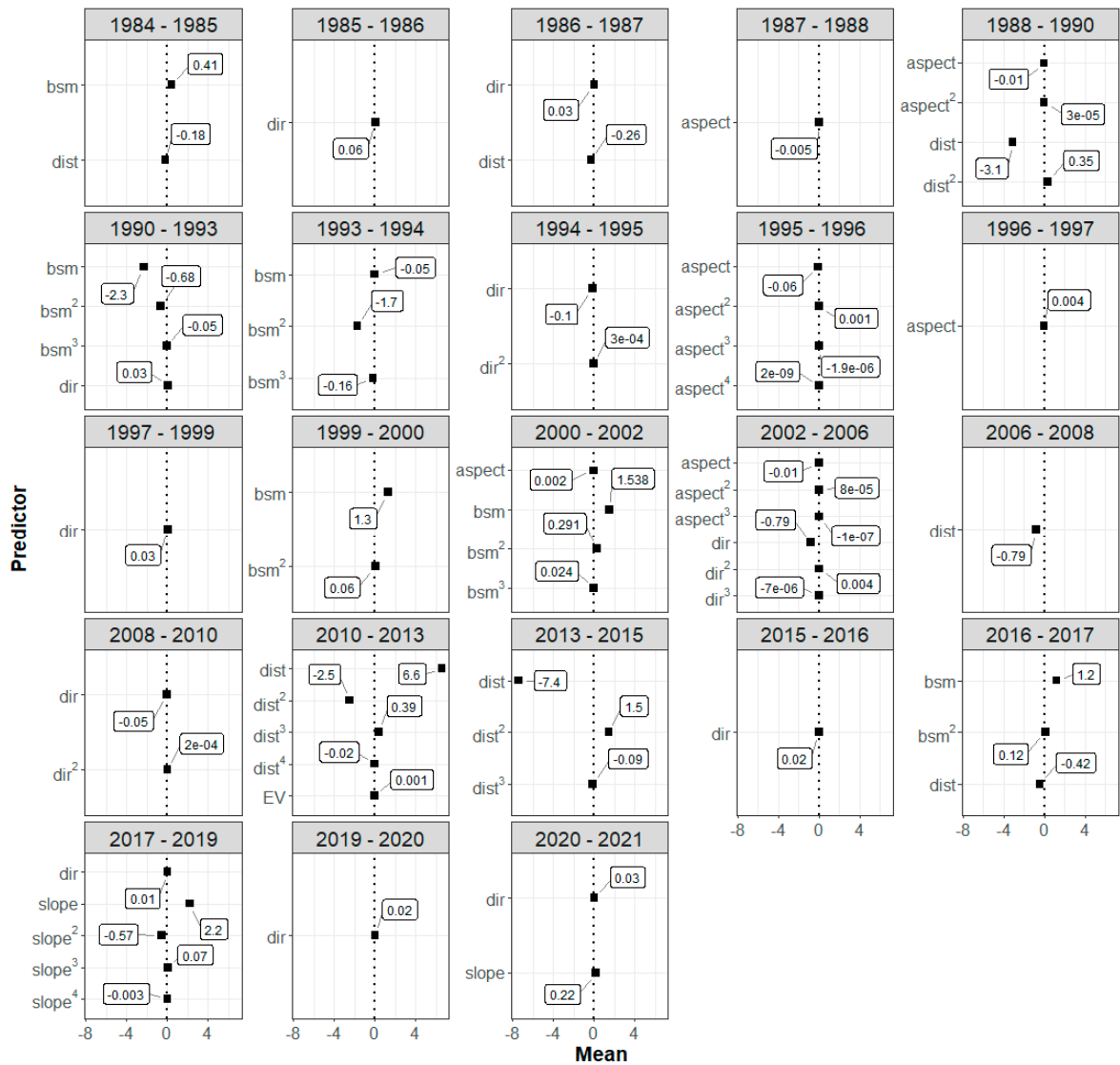


Figure 8. Individual plots of the mean of the parameter estimate (represented as closed (black) squares and the values are presented in rectangles) for the most important spatial pattern predictors of SAV loss in the Bluefields Bay Special Fish Conservation Area (BBSFCA), Westmoreland, Jamaica for 23 successive 1-to-4-year periods between 1984 – 2021. The values were generated from the final parsimonious Bayesian Integrated Nested Laplace Approximation (INLA) models. dist and dir = distance and direction from the mouth the main river that empties in the bay; EV = average exposure vulnerability for two hurricanes (Ivan and Dean).

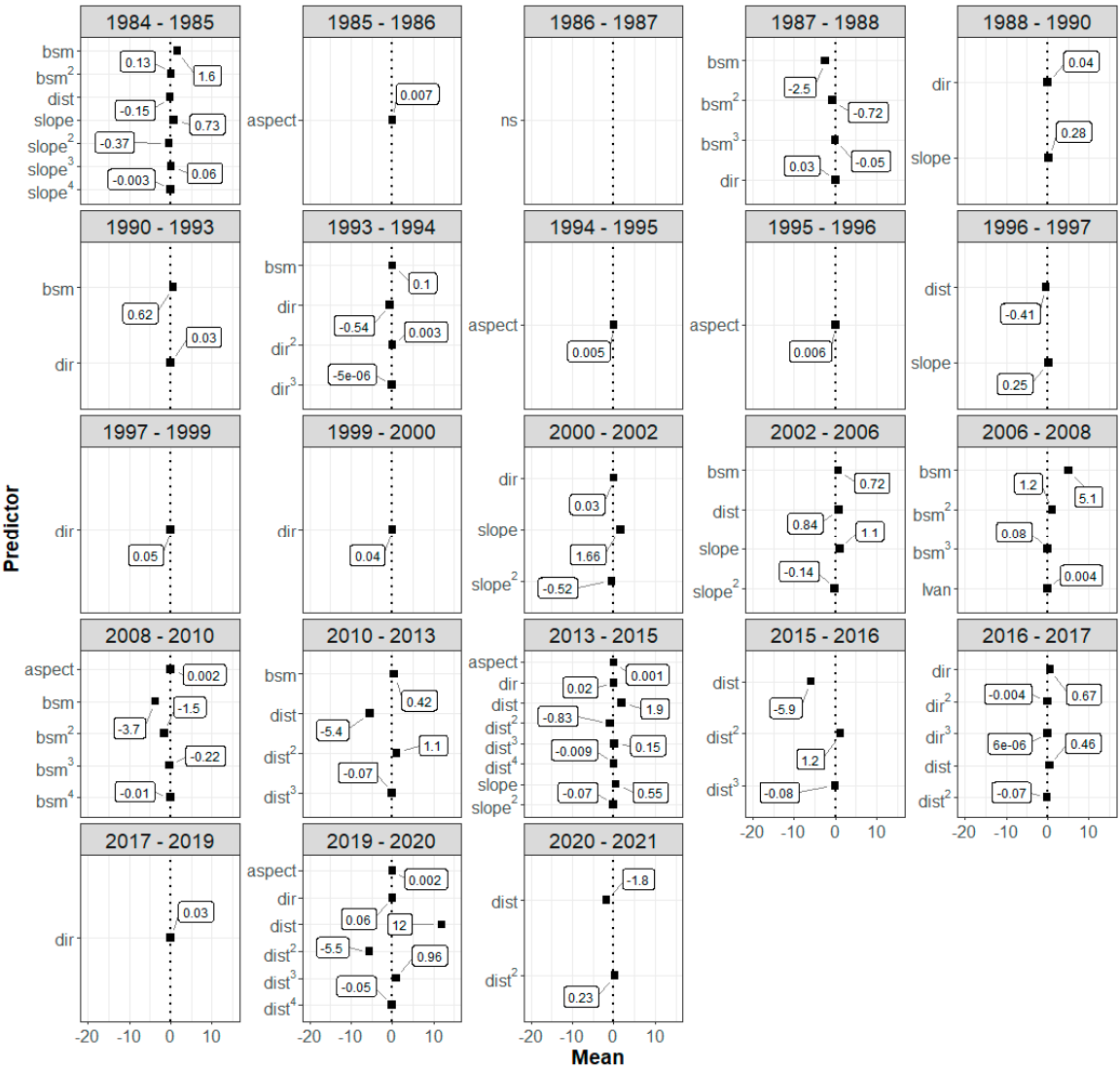


Figure 9. Individual plots of the mean of the parameter estimate (represented as closed (black) squares and the values are presented in rectangles) for the most important spatial pattern predictors of SAV gain in the Bluefields Bay Special Fish Conservation Area (BBSFCA), Westmoreland, Jamaica for 23 successive 1-to-4-year periods between 1984 – 2021. The values were generated from the final parsimonious Bayesian Integrated Nested Laplace Approximation (INLA) models. dist and dir = distance and direction from the mouth the main river that empties in the bay; Ivan = exposure vulnerability for Hurricane Ivan.

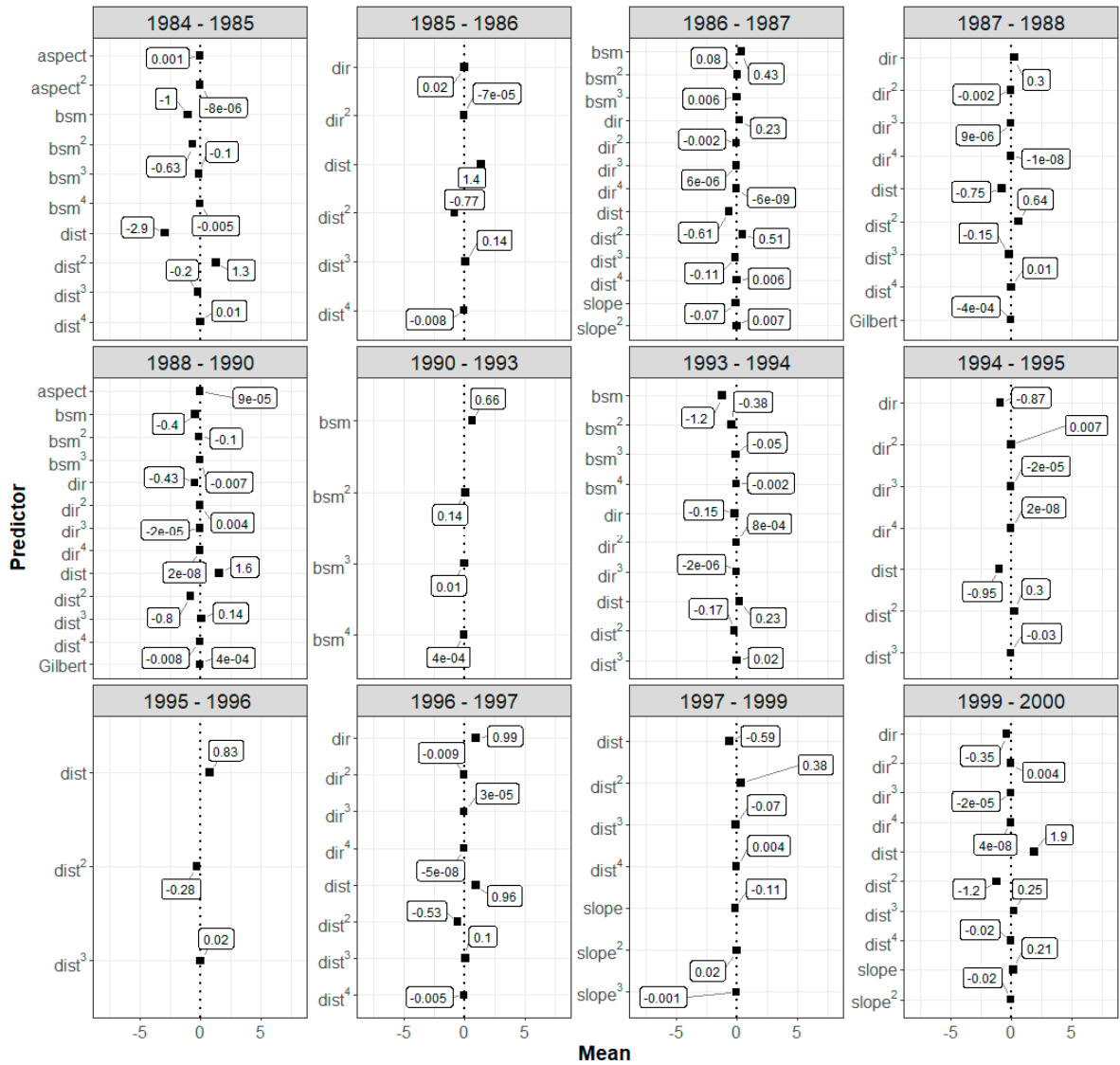
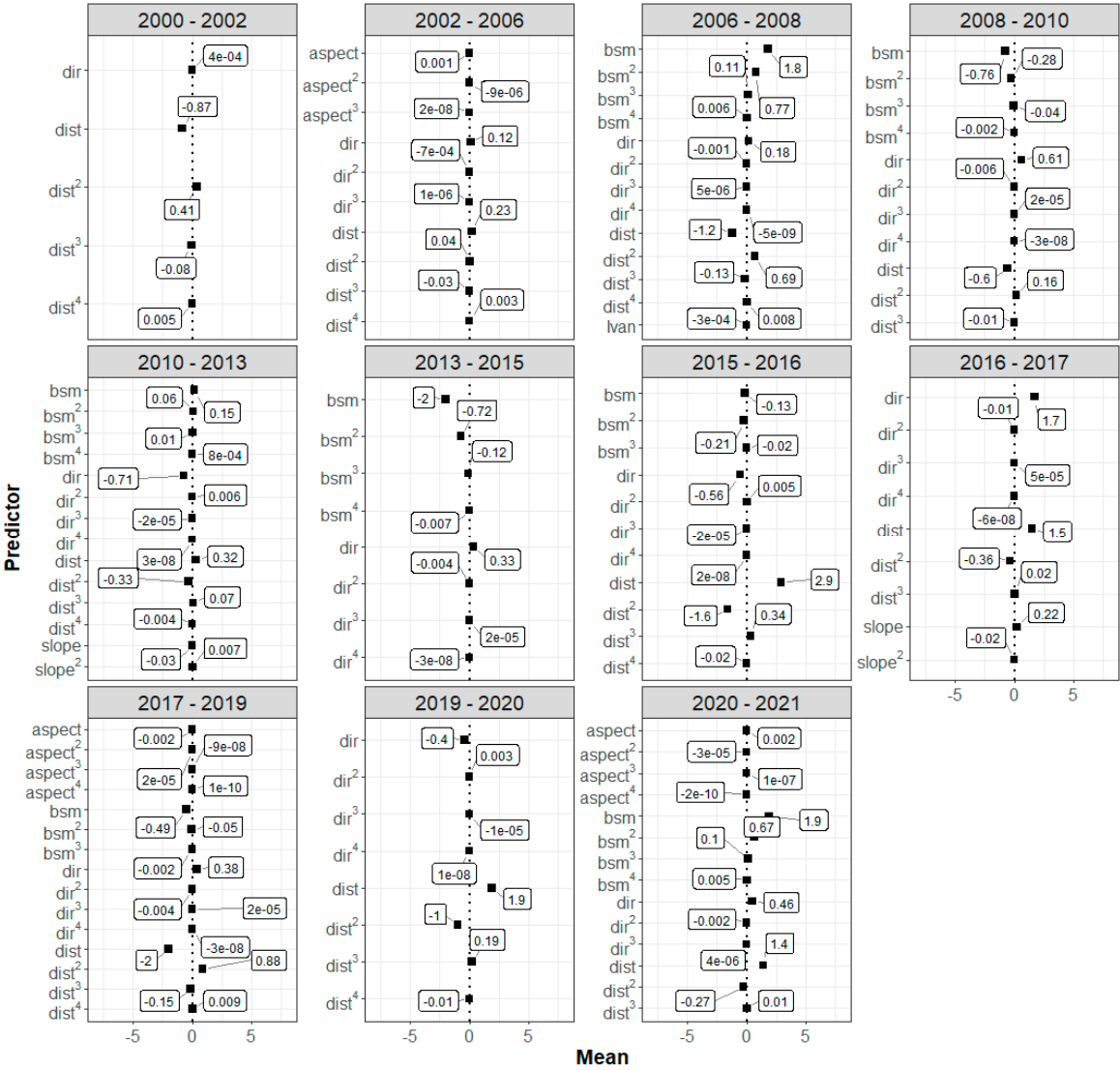


Figure 10. Individual plots of the mean of the parameter estimate (represented as closed (black) squares and the values are presented in rectangles) for the most important spatial pattern predictors of SAV percentage cover change in the Bluefields Bay Special Fish Conservation Area (BBSFCA), Westmoreland, Jamaica for 12 successive 1-to-4-year periods between 1984 – 1999. The values were generated from the final parsimonious Bayesian Integrated Nested Laplace Approximation (INLA) models. dist and dir = distance and direction from the mouth the main river that empties in the bay; Gilbert = exposure vulnerability for Hurricane Gilbert.



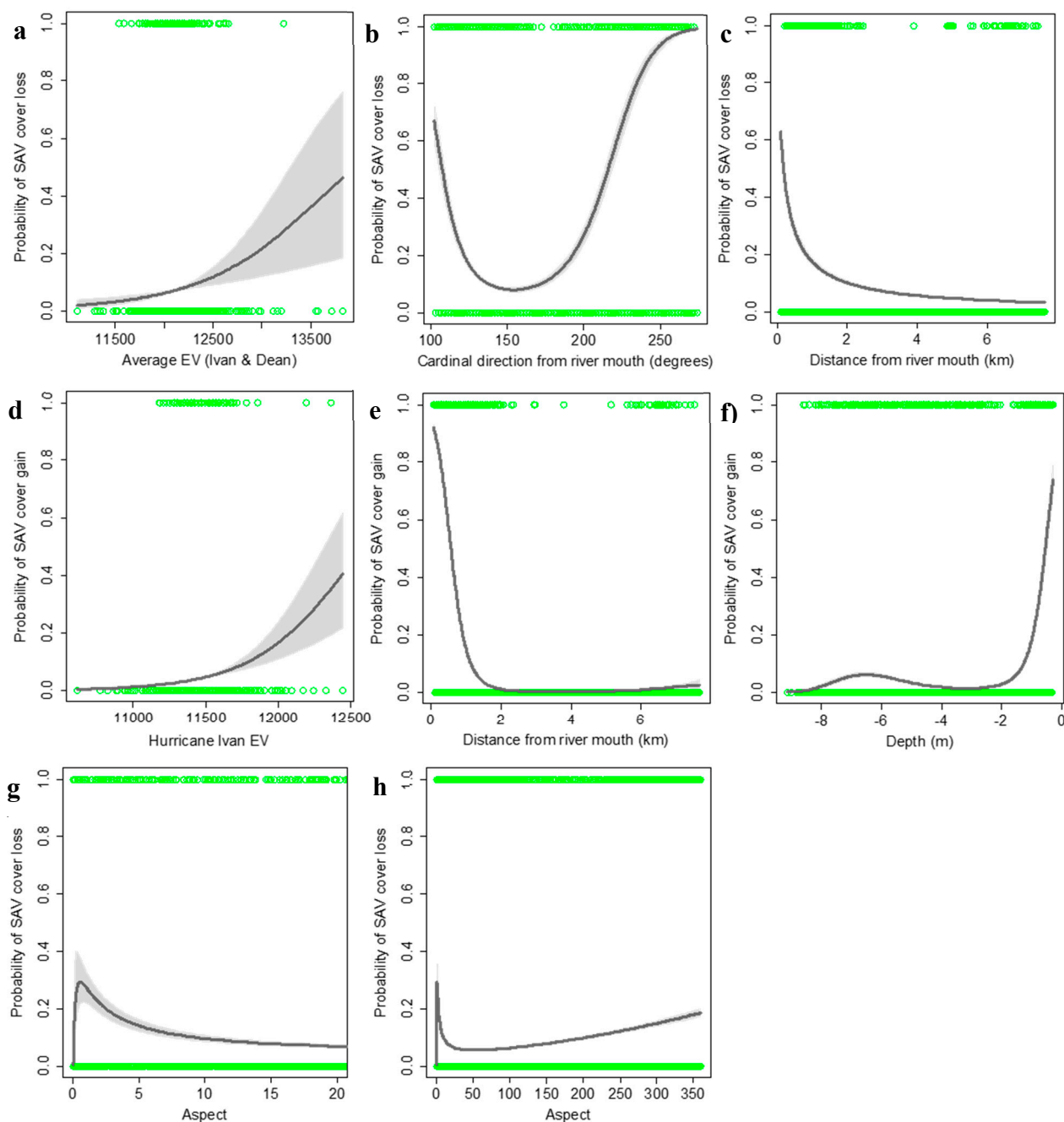


Figure 12. Observed and predicted values obtained from Bayesian Integrated Nested Laplace Approximation (INLA) models that included several important predictors of SAV loss and gain (probability) in the Bluefields Bay Special Fish Conservation Area (BBSFCA), Westmoreland, Jamaica. These include SAV loss and a) average exposure vulnerability (EV) for Ivan and Dean (2010 – 2013), b) cardinal direction from river mouth (2002 – 2006) and c) distance from river mouth (2006 – 2008). Also included is SAV gain and d) Hurricane Ivan EV (2006 – 2008), e) distance from river mouth (2010 – 2013) and f) depth (2006 – 2008) and g – h) SAV loss and two different ranges of aspect (degrees) values to highlight peak aspect values. Grey shade = standard error.

Marginal R-squared values for the predictors of SAV cover gain ranged from 0.04% – 37.2%, with the highest value being obtained during the 2010 – 2013 period (Figure 7) when SAV cover was recovering following the passage of two hurricanes. A single predictor of SAV gain was found to be important during 8 of the 23 periods assessed, whereas multiple predictors were important for the remaining periods (Figure 9). Additionally, there were no important predictors for SAV gain during

one period (1986 – 1987). Also, the most important predictors had a positive or a negative effect on SAV gain, and the influence of the predictors were best explained by linear or polynomial relationships (Figures 9 and 12d–f). Like SAV loss, SAV gain was most frequently predicted by direction and distance (11 and 9 intervals, respectively) followed by BSM, aspect, slope, and Hurricane Ivan EV (8, 6, 6 and 1 intervals, respectively) (Figure 9). These results again highlighted that proximity to the mouth of the river influenced dynamic changes. Specifically, SAV gain was positively related to the direction from the river mouth for 9 of 11 periods when the latter was important and like SAV loss, indicating that the highest probability of gain occurred largely to the southwest to northwest of the river mouth. Also, SAV loss was higher closer to the river mouth during 5 of 9 intervals. The probability of SAV gain was highest at shallow locations (6 of 8 periods, e.g. Figure 12f) than at greater depths (only 2 periods) (Figure 9). Moreover, there was greater SAV gain where Hurricane Ivan EV was highest during the period (2006 – 2008) (Figures 9 and 12d) that followed the passage of Ivan in 2004, indicating that SAV cover was recovering at sites that were impacted by Ivan but not by Dean.

Marginal R-squared values for the predictors of percentage cover change ranged from 8.3% – 54.7%, with the highest value being obtained during the 2015 – 2016 period (Figure 7). Also, multiple predictors were largely found to be important (Figures 10 and 11). The most common relationship was polynomial indicating that the influence of the predictors varied across the range of values for the predictors, and again the relationships can either be positive or negative (Figures 10, 11 and 13a–f). The most frequent important predictors were distance and direction from the river mouth (21 and 19 intervals, respectively). This was followed by BSM, slope, aspect, and EV (12, 5, 5 and 3 intervals, respectively). Unlike SAV loss and gain, percentage cover change may have been influenced by hurricanes three times (Figures 10, 11 and 13a,b). Hurricane Gilbert EV negatively influenced SAV percentage cover change during the period when Gilbert made landfall (1987 – 1988) but this changed to positive relationship during the period after the hurricane (1988 – 1990), indicating the recovery of SAV cover at high EV areas (Figures 10 and 13a,b). Hurricane Ivan EV had a negative influence when other predictors influenced SAV percentage cover change during the period after the hurricane passed the island (2006 – 2008), which is possibly a lag effect (Figures 11).

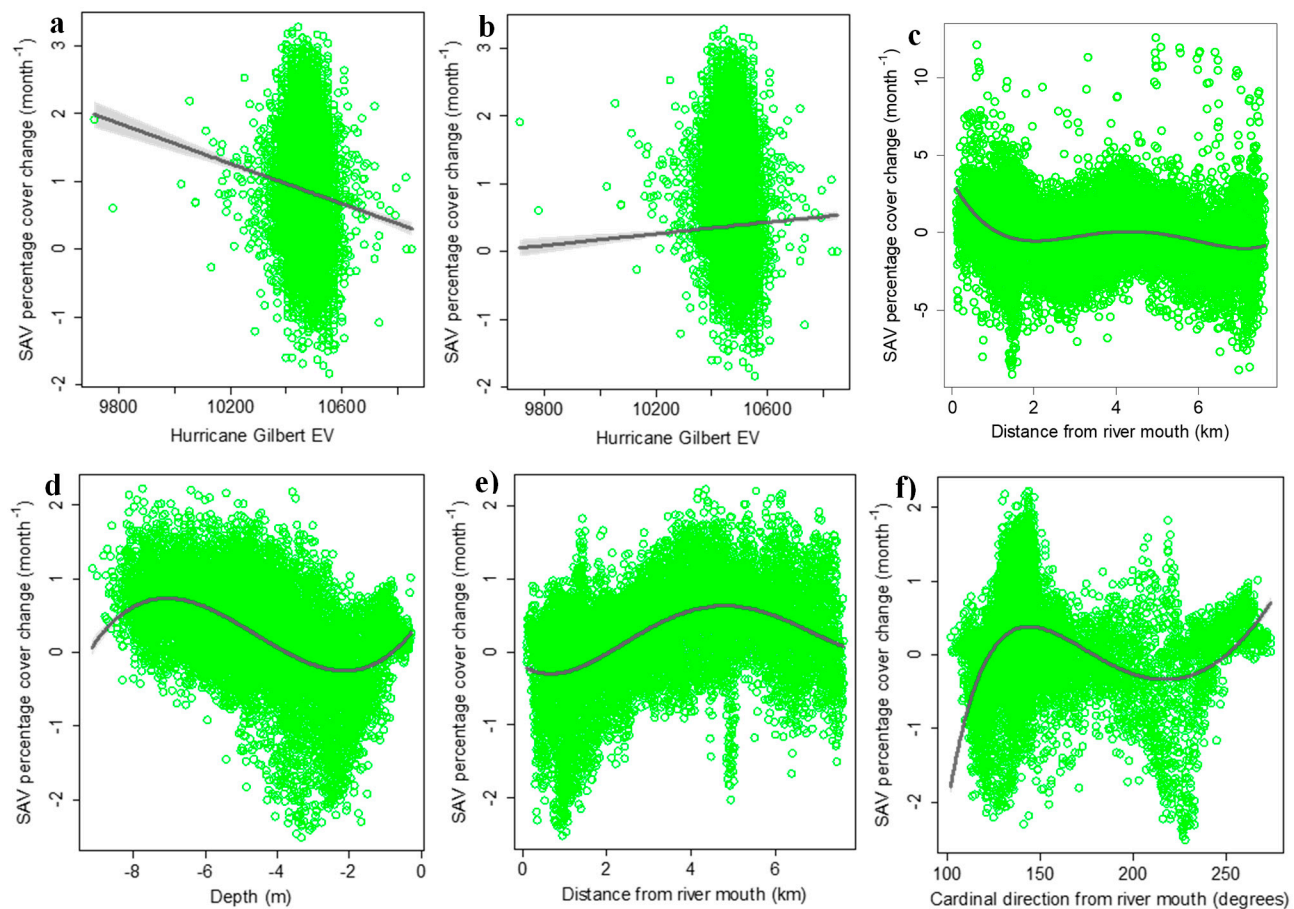


Figure 13. Observed and predicted values obtained from Bayesian Integrated Nested Laplace Approximation (INLA) models that included several important predictors of SAV percentage cover change (monthly) in the Bluefields Bay Special Fish Conservation Area (BBSFCA), Westmoreland, Jamaica. These include SAV percentage cover change and a - b) Hurricane Gilbert exposure vulnerability (EV) (1987 – 1988 and 1988 – 1991, respectively), c) distance from river mouth (1984 – 1985), d) depth (2006 - 2008), e) distance from river mouth and f) cardinal direction from river mouth (2006 - 2008). Grey shade = standard error.

4. Discussion

In this study, we identified various factors that influenced SAV extent and percentage cover over a period of 37 years. We used data and maps generated from a random forest regression model that used 2013 hydroacoustic data to predict SAV percentage cover from reflectance data from 24 Landsat satellite images that were collected during the period 1984 - 2021. Our assessments were based on several assumptions. We used level 2 processed images with atmospheric correction, which should standardize the reflectance data for each image. This is important as we were not able to determine the accuracy of the SAV percentage cover maps generated for the years before or after 2013. Because the images were standardized, it is expected that the reflectance values would fall within a similar range and therefore the SAV percentage cover maps should have similar accuracies. We also made this assumption when using/applying thresholds for converting SAV percentage cover to binary, that is, the thresholds would produce maps with similar accuracies to our 2013 thematic maps. Nevertheless, we were able to use the resulting maps/data from the maps to identify how several factors influenced seagrass cover change at our study site.

4.1. Spatial pattern predictors of SAV change

There have been reported declines in seagrass cover due to a variety of factors including natural hazards such as single [18] or multiple storms/cyclones/hurricanes [17], droughts [21], a combination of droughts and storms/cyclones/hurricanes [70]; [21], a combination of storms and cyclones and above average rainfall [71] and due to anthropogenic activities despite protection [23]. However, several studies have reported stable SAV cover [72] or an expansion/increase in SAV area due to increased protection [9] or despite the impacts of multiple storms [20]. We found that seagrass percentage cover and extent in the BBSFCA were largely stable over the 37-year period and SAV loss and gain for several periods were explained by proximity to the mouth of a river. The spatial pattern analysis using the pixel-based regression and the spatial Bayesian INLA models confirmed that an area of active/dynamic change can be found close to the mouth of the river, towards the western side of the bay. We found that annual rainfall was at historic lows and higher monthly rainfall had a positive influence on seagrass percentage cover. The pixel-based regression confirmed the latter, specifically that overall, higher rainfall largely had a positive influence on SAV gain and percentage cover change. This is contrary to the findings of several studies that have reported that higher rainfall results in increased surface runoffs or outflows from rivers into bays, and this is generally associated with increased turbidity and nutrients, which increases SAV stress and reduces extent or cover (e.g. [73]) and vertical growth [74]. Flood outflows can increase these impacts significantly (e.g., a 2 – 3-fold increases in turbidity and nutrients) resulting in an even greater decline in seagrasses [75]. Droughts can result in increased evaporation of water and salinity (creating hypersaline conditions) and bottom-water anoxia, leading to a reduction in SAV cover and extent (e.g. [19]), particularly during low tides in intertidal areas (e.g. [76]). Also, seasonal rainfall is associated with lower and higher SAV percentage cover/extent during the wet and dry seasons, respectively (e.g. [73,77]). Our result is therefore unusual, and even after reviewing studies of freshwater SAVs (e.g. [78]), higher rainfall has not been reported to be associated with an increase in SAV percentage cover and/or extent. Higher rainfall does result in increased turbidity in the BBSFCA, as we were not able to use images collected during several years because of high turbidity around the mouth of the river, or across most of the western half of the bay. Also, the predominant sediment type found in the persistently bare area to the west of the bay (and the mouth of the river), and close to the coastline is silt [30], indicating that there is a constant input of terrigenous sediment. However, we did not examine the effects of monthly rainfall using seagrass cover data collected every month (e.g. [73]). Instead, we calculated monthly rates of percentage cover change, and recorded SAV loss and gain using images captured over a minimum period of 4 months to a maximum period of 46 months, due to the unavailability of suitable images. Also, rainfall in Jamaica and on the south coast is seasonal; therefore, we likely captured the overall response of SAVs to rainfall irrespective of seasons, that is, before, after or during one or more wet and/or dry seasons. Nevertheless, seagrass meadows/beds have been found to be nutrient limited [79,80], and therefore, moderate increases in nutrients are beneficial [81] - high inputs, however, are detrimental as it promotes the growth and dominance of competing macroalgae [81,82]. Additionally, although there have been reported declines in seagrass percentage cover during wet seasons, this can be followed by rapid recovery during the following dry season [73]. Furthermore, nutrients that are brought by outflows or runoffs during the rainy season is thought to contribute to the recovery of seagrass percentage cover during the dry season that follows the rainy season [73]. This can perhaps be used to explain our results. That is, over time SAV in the bay benefitted from higher overall inputs of nutrients from outflows during the rainy season. Moreover, the bay is currently receiving < 1000 mm of the total annual rainfall it received at the turn of the 20th century, yet SAV extent was largely maintained, and percentage cover in most of the bay was > 80%, 6 out of the 24 times it was mapped, the most recent being in 2019. It is conceivable that the bay might be receiving less nutrients than it did over 100 years ago, especially during periods of low rainfall. However, there has been extensive agricultural (along the river course) and coastal developments and perhaps this is compensating for a reduction in nutrient inputs. We are currently investigating whether the positive effect of rainfall is maintained when images with higher temporal and spatial resolutions are used.

There was a significant decline in SAV area/extent during one period, 2002 – 2006, when the island was impacted by Hurricane Ivan. The effects of Ivan may have been compounded by a second hurricane (Dean), three years later (Figure A4). As a result, SAV extent/area did not fully recover until the 2013 – 2015 period, or 9 – 11 years after the impact of the first hurricane. The identified important spatial pattern predictors can be used as evidence for the impact of Ivan and Dean; specifically, direction from the mouth of the river and aspect were the most important predictors of SAV loss during the 2002 – 2006 period. For the first of the two predictors, this was the first time that the probability of SAV loss was equally high on both sides of or multiple cardinal directions from the mouth of the river (southeast and southwest to the northwest; Figures 8 and A3), indicating that there was a higher than usual outflow from the river. This may have influenced SAV loss, due to exceedingly high rainfall during hurricane events, which can be detrimental to seagrass beds [83]. The net effect was an increase in the extent of the SAV absent class around the mouth of the river, which for the first time extended from the southwest and west to the southeast of the river mouth (Figure 3). Also, percentage cover around the river fell to $\leq 20\%$ for the first time (Figure 2). Following the hurricanes, direction or distance from the river mouth was an important predictor of SAV loss for every period until 2013 – 2015, during which, the size of the SAV absent class close to the river increased (Figures 3 and 8). SAV did not recolonize the newly transformed SAV absent areas until 2015 (Figures 3 and 8). The second important predictor, aspect, was used in the calculation of EV, and it is a proxy to the predominant direction of exposure to hurricane winds [36,52]. It can also confound the influence of EV as it can be a more important predictor of hurricane damage if the impact of a hurricane is strong in a given/particular direction because the winds are moving predominantly in that direction [52]. Our results showed that SAV loss was greatest at areas on the benthos that had a northwestern to northern facing aspect (Figures 12g,h and A3). This corresponded with the prevailing wind direction of the leading edge (the most destructive/strongest winds) of the outer wind bands of Ivan (Figure A4). Several studies that have employed the use of wave models have reported similar directional impacts of storms on seagrass beds/meadows; these impacts were also associated with the prevailing direction of the storms' winds (e.g. [84,85]). Also, seagrass declines following storms are usually associated with persistent changes in seawater quality and burial [86]. Greater exposure to the direction of the prevailing winds of a storm was one of two factors that explained the depth of burial of seagrasses found along the Spanish Mediterranean coast (higher exposure to storm winds increased burial depths) that were impacted by Storm Gloria in 2020 [85]. Burial may have been the main impact of Ivan as there were several bare sand patches present during the 2006 – 2013 period (Figure 3), one of which was described as a "sand bar" by [30]. These bare patches were not present in the maps of benthic classes before 2006 or after 2013 (Figure 3). The "sand bar" first appeared in the south-eastern section of the bay in 2006 in an area previously covered by seagrass (Figure 3). By 2015 however, the "sand bar" and all the bare sand patches were recolonized and were no longer visible in the benthic features maps (Figure 3).

We also found evidence of the cumulative impact of two hurricanes that follow similar tracks. The first evidence was that there was SAV gain/recovery and positive SAV percentage cover change at some sites on the benthos during 2006 – 2008, which were exposed to Hurricane Ivan in 2004, and this recovery/change preceded a complete recovery of all impacted areas/sites in 2015. These were likely to be sites/locations that were impacted by Ivan in 2004, but not by Dean in 2007 and were recovering during this period, while other areas impacted by both hurricanes continued to experience a loss up until 2013. Moreover, the cumulative effects of Ivan and Dean (average EV) explained (although the marginal R-squared was low) the pattern of SAV loss (higher average EV was associated with a higher probability of loss) during 2010 – 2013, 9 and 6 years after Ivan and Dean, respectively, impacted our study site. This likely contributed to the (relatively) long period it took for SAV extent/area to recover (close to decade). The cumulative negative impacts of storms have been reported elsewhere. For example, on the southwestern coast of Korea, the cumulative effects of three consecutive typhoons in two months, resulted in a seagrass meadow completely dying off, despite previous (single) typhoons having little or no impact [17]. The contrasting impacts of previous single typhoons versus the three consecutive typhoons also indicate that the damage caused by storms,

hurricanes, cyclones, or typhoons can be very variable and range from no damage to complete degradation, die-off, or habitat destruction [20,86]. We also found that the impacts of different hurricanes on SAV in the BBSFCA can vary. While Ivan and Dean impacted SAV extent, Hurricane Gilbert did not have a similar impact, but instead may have reduced seagrass percentage cover during the period 1987 - 1988, and it recovered immediately during the period that followed (1988 - 1990). Similarly, the short-term impacts of a cyclone on seagrasses in southwestern Madagascar included a decline in percentage cover and height [18]. Our observed differences in impact may be explained by the tracks of the hurricanes (and distance of the eye from the island). The strongest winds or leading edge of hurricanes with a track close to the south of Jamaica will cover most of the island, tend to have a predominantly northern wind direction, and will have a greater impact on the south coast (Figure A4). Hurricane Gilbert made landfall and as such, the proxy hurricane indicated that the leading edge of the hurricane would have been largely offshore to the north of the island, with only the trailing weaker wind bands affecting the BBSFCA on the south coast (Figure A4). These patterns of impact mirror the impacts of hurricanes on forest ecosystems in Jamaica, where the track and distance of the eye of a hurricane from the island (and whether they pass to the south, north or make landfall) can be used to determine the sites/locations that experienced the greatest impacts [36].

Depth and benthic topography have been previously reported as being important predictors of seagrass presence, density, or percentage cover, but there is a paucity of studies on how they influence dynamic changes. Seagrasses were found to colonize a gentle slope with an inclination of 0.0 to 56.6 degrees along the coast of Giglio Island, Italy [24]. Also, seagrass cover increased with higher slope values and depth in shallow areas [24]. Shoot density decreased non-linearly with depth with peak densities being found at intermediate depths in a fringing-reef lagoon in the Mexican Caribbean [87]. Additionally, seagrass distribution in shallow water can be limited by exposure to wind and wave, or where exposure to waves is greater, whereas in deeper water they are limited by light [87,88]. As stated previously, aspect can give an indication of directional impact or areas predominantly exposed to a specific wave/wind direction. For the BBSFA, the average slope percentage, aspect and depth were 0.8% (or equivalent to 0.4 degrees), 206 degrees or a predominant southwestern facing aspect, and 4.2 m (range: 0.05 – 9.3 m), respectively. SAV was present across the entire bay over our study period and therefore was not limited by depth or benthic topography. However, we found that the probability of SAV loss and gain were higher in shallow areas, mainly around the mouth of the river, indicating that these were areas of dynamic change in the BBSFCA. High sediment input and greater exposure to wave action and wind, may have influenced dynamic changes in these areas. Some shallow areas, however, may have been impacted by anthropogenic activities, as there was a large beach and other smaller public beaches and several beaches associated with lower impact coastal developments (small higher end resorts) found in shallow areas along the coast. Slope and aspect were the least selected benthic topographic predictors of spatial pattern change. Topographic variation was subtle in this bay, and this perhaps can explain the low importance of slope and aspect. Nevertheless, aspect was an important indicator of/proxy to Hurricane Ivan impact.

4.1. Implications for management

SAV cover was stable before and continued to be stable after the BBSFCA was established. Consequently, the BBSFCA is working, that is, it is helping to maintain SAV cover. The main area of dynamic change was around the mouth of the main river that drains into the bay, with one area towards the west end of the bay being consistently bare. Under normal circumstance we would recommend that the BBSFCA managers integrate land-sea or ridge-to-reef conservation planning [10–12] to address the threat posed by high terrigenous sediment load in river outflows. But this might be beyond the remit of the present managers. Additionally, rainfall, and hence river outflow, may be important due to its positive impact on SAV loss, gain, and percentage cover change, and given the significant reduction in annual rainfall. Moreover, hurricanes pose the greatest threat to the maintenance of SAV cover. We showed that the cumulative impacts of two hurricanes that followed a similar track to the south of the island can reduce SAV extent for an extended period. Even

a single hurricane that made landfall and had less of an impact (Hurricane Gilbert) can reduce percentage cover. The island was impacted by four hurricanes in 8 years (Hurricanes Ivan (2004), Dennis (2005), Dean (2007) and Sandy (2012)), but only two of the four hurricanes passed to the north of island. In the future, successive hurricanes that pass to the south of the island will have the capacity to substantially reduce SAV cover. Depth was found to be an important predictor of SAV dynamic change, and although this was primarily limited to shallow areas around the river mouth, loss may also be occurring in shallow areas with high anthropogenic activity (beaches and coastal developments). This, however, will need to be verified and there is also a need to further verify the positive effect of rainfall using data with higher temporal and spatial resolutions. If the latter is found to be important, a further reduction in rainfall will also have serious implications for management.

5. Conclusions

We were able to document changes in SAV extent and percentage cover in the BBSFCA over a period of 37-years using data from 24 percentage cover and benthic features maps. These maps were generated by first building a random forest regression model with 2013 percentage cover hydroacoustic data (dependent variable) and reflectance data from 2013 Landsat 7 and 8 satellite images and auxiliary data as the predictors and then using the model to predict percentage cover using data from the Landsat satellite series. A threshold was applied to the percentage cover maps to generate the benthic features maps. We demonstrated that SAV cover was quite stable and possibly quite healthy with several years with >80% percentage cover over most of the bay. There was a significant loss in SAV area between 2006 –2013, with a subsequent recovery in 2015. We found that this loss may have initially occurred due to the impact of Hurricane Ivan in 2004, and this was compounded by a second hurricane (Dean) in 2007, which may have delayed the recovery of SAV extent until a decade after Ivan. Rainfall, and by extension outflow from the main river that drains into the bay, had an overall positive effect and is contributing significantly to SAV loss, gain, and percentage cover change, despite annual rainfall being approximately 1000 mm less on average than it was at the turn of the 20th century. We surmised that a loss of nutrient input caused by reduced outflows may have been supplemented by increased nutrient loads from agricultural and coastal developments. Shallow areas around the river mouth, and possibly areas close to coastal developments and beaches were also active areas of change. An increase in the frequency of high intensity hurricanes and an increase in the variability of rainfall in Jamaica, which can perhaps explain a reduction in annual rainfall at the BBSFA, will impact the site in the future.

Supplementary Materials: The following supporting information can be downloaded at the website of this paper posted on Preprints.org. **Table S1:** Validation criteria for finals models that included the most important predictors of the probability of submerged aquatic vegetation (SAV) loss in the Bluefields Bay Special Fish Conservation Area (BBSFCA), Westmoreland, Jamaica, for 23, 2 – 4-year periods, generated using a 5-fold cross validation of spatial Bayesian Integrated Nested Laplace Approximation (INLA) generalized linear mixed models. The validation criteria used included: mean squared error (MSE), root mean squared error (RMSE), mean absolute error (MAE), mean absolute percentage error (MAPE), bias (a measure of consistent under- or over-forecasting; BIAS), relative bias (rBIAS), and relative mean separation (rMSEP). Also included are the calculated values for the receiver operating characteristic (ROC) curve (AUC), deviance information criterion (DIC), and marginal R-squared (mR2); **Table S2:** Validation criteria for finals models that included the most important predictors of the probability of submerged aquatic vegetation (SAV) gain in the Bluefields Bay Special Fish Conservation Area (BBSFCA), Westmoreland, Jamaica, for 23, 2 – 4-year periods, generated using a 5-fold cross validation of spatial Bayesian Integrated Nested Laplace Approximation (INLA) generalized linear mixed models. The validation criteria used included: mean squared error (MSE), root mean squared error (RMSE), mean absolute error (MAE), mean absolute percentage error (MAPE), bias (a measure of consistent under- or over-forecasting; BIAS), relative bias (rBIAS), and relative mean separation (rMSEP). Also included are the calculated values for the receiver operating characteristic (ROC) curve (AUC), deviance information criterion (DIC), and marginal R-squared (mR2); **Table S3:** Validation criteria for finals models that included the most important predictors of submerged aquatic vegetation (SAV) percentage cover change in the Bluefields Bay Special Fish Conservation Area (BBSFCA), Westmoreland, Jamaica, for 23, 2 – 4-year periods, generated using a 5-fold cross validation of spatial Bayesian Integrated Nested Laplace Approximation (INLA) generalized linear

mixed models. The validation criteria used included: mean squared error (MSE), root mean squared error (RMSE), mean absolute error (MAE), mean absolute percentage error (MAPE), bias (a measure of consistent under- or over-forecasting; BIAS), relative bias (rBIAS), and relative mean separation (rMSEP). Also included are the calculated values for the deviance information criterion (DIC), and marginal R-squared (mR2).

Author Contributions: Conceptualization, methodology, validation, formal analysis, investigation, and resources, Kurt McLaren; Hydroacoustic data collection and processing, Karen McIntyre, Kurt Prospere, and Kurt McLaren; writing—original draft preparation, Kurt McLaren and Jasmine Sedman; writing—review and editing, visualization, and supervision, Kurt McLaren. All authors have read and agreed to the published version of the manuscript.

Funding: This research received no external funding.

Data Availability Statement: Data available upon request from the corresponding author.

Conflicts of Interest: The authors declare no conflict of interest.

Appendix A

Table A1. List of Landsat satellite images that were used in this study.

Name of File	Landsat Series	Path	Row	Date
LT05_L2SP_012047_19841009_20200918_02_T1	Landsat 4-5	12	47	09/10/1984
LT05_L2SP_012047_19850302_20200918_02_T1	Landsat 4-5	12	47	02/03/1985
LT05_L2SP_012047_19860217_20200918_02_T1	Landsat 4-5	12	47	17/02/1986
LT05_L2SP_012047_19870628_20201014_02_T1	Landsat 4-5	12	47	28/06/1987
LT04_L2SP_012047_19880926_20200917_02_T1	Landsat 4-5	12	47	26/09/1988
LT05_L2SP_012047_19900503_20200915_02_T1	Landsat 4-5	12	47	03/05/1990
LT04_L2SP_012047_19930111_20200914_02_T1	Landsat 4-5	12	47	11/01/1993
LT05_L2SP_012047_19940223_20200913_02_T1	Landsat 4-5	12	47	23/02/1994
LT05_L2SP_012047_19950330_20200912_02_T1	Landsat 4-5	12	47	30/03/1995
LT05_L2SP_012047_19960316_20200911_02_T1	Landsat 4-5	12	47	16/03/1996
LT05_L2SP_012047_19970404_20200910_02_T1	Landsat 4-5	12	47	04/04/1997
LT05_L2SP_012047_19991019_20200907_02_T1	Landsat 4-5	12	47	19/10/1999
LE07_L2SP_012047_20000131_20200918_02_T1	Landsat 4-5	12	47	31/01/2000
LE07_L2SP_012047_20021120_20200916_02_T1	Landsat 7	12	47	20/11/2002
LE07_L2SP_012047_20060304_20200914_02_T1	Landsat 7	12	47	04/03/2006
LE07_L2SP_012047_20060421_20200914_02_T1	Landsat 7	12	47	21/04/2006
LT05_L2SP_012047_20080520_20200829_02_T1	Landsat 4-5	12	47	20/05/2008
LT05_L2SP_012047_20100118_20200825_02_T1	Landsat 4-5	12	47	18/01/2010
LE07_L2SP_012048_20130510_20200907_02_T1	Landsat 7	12	48	10/05/2013
LE07_L2SP_012047_20131017_20200907_02_T1	Landsat 7	12	47	17/10/2013
LC08_L2SP_012047_20131126_20200912_02_T1	Landsat 8	12	47	26/11/2013
LC08_L2SP_012047_20150116_20200910_02_T1	Landsat 8	12	47	16/01/2015
LC08_L2SP_012047_20160220_20200907_02_T1	Landsat 8	12	47	20/02/2016
LC08_L2SP_012047_20170222_20200905_02_T1	Landsat 8	12	47	22/02/2017

LC08_L2SP_012047_20190111_20200830_02_T1	Landsat 8	12	47	11/01/2019
LC08_L2SP_012048_20200318_20200822_02_T1	Landsat 8	12	48	18/03/2020
LC08_L2SP_012047_20210422_20210430_02_T1	Landsat 8	12	47	22/04/2021

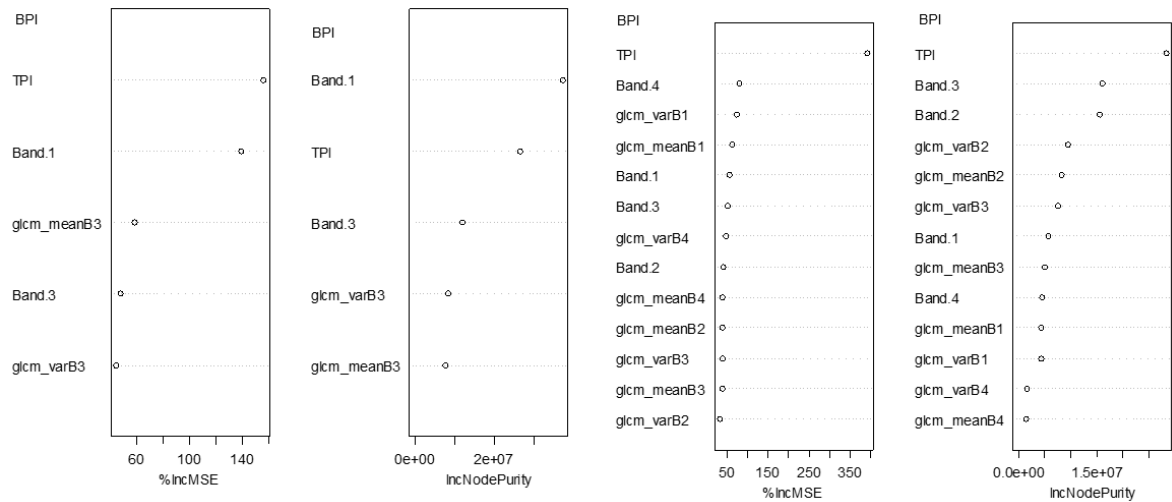


Figure A1. Random forest predictor importance plots for random forest regressions that were used to model the relationship between hydroacoustic submerged aquatic vegetation (SAV) percentage cover training data (78% of the SAV data or 107,076 data points) and several predictors including bathymetric position index [BPI] data and band reflectance and Grey Level Co-Occurrence Matrix (GLCM) mean (glcm_mean) and variance (glcm_var) data from Landsat images for the year 2013, for a) bands 1 (Band 1 or B1) and 3 (Band 3 or B3) from a composite Landsat 7 image with the missing data filled in and b) bands 1 – 4 (Band 1...Band 4 or B1...B4) for a Landsat 8 image. The randomForest package uses %IncMSE and IncNodePurity in a regression tree analysis to rank predictor importance. The %IncMSE is the percentage increase in mean square error (MSE) of predications, estimated using the out of bag coefficient of variation. A higher %IncMSE value represents a higher variable importance (large percentage increase in MSE if the variable is removed) and conversely, lower importance indicates small changes in MSE when the predictor is added or removed. IncNodePurity is the increase in data partition homogeneity.

Table A2. Measures of accuracy calculated for two random forest regression models (RFr) that were used to model the relationship between hydroacoustic submerged aquatic vegetation (SAV) percentage cover data and several predictors including bathymetric position index [BPI] data and band reflectance and Grey Level Co-Occurrence Matrix (GLCM) mean and variance data from Landsat images for the year 2013, for bands 1 and 3 from a composite Landsat 7 image with the missing data filled in and bands 1 – 4 for a Landsat 8 image. The testing data accounted for 12% of the SAV data or 14,853 data points. Accuracy measures include mean squared error (MSE), root mean square error (RMSE), mean absolute error (MAE), mean absolute percentage error (MAPE), bias (BIAS), relative bias (rBIAS), and relative mean separation (rMSEP). Var (%) = percentage variance explained by the model.

RFr models	Var (%)	MSE	RMSE	MAE	MAPE	BIAS	rBIAS	rMSEP
SAV x BPI + Landsat 7 reflectance and GLCM data	62.7	656.5	25.6	19.2	39.1	1.3	0.0202	0.4
SAV x BPI + Landsat 8 reflectance and GLCM data	69.8	595.2	24.4	17.7	37.7	0.1	0.0008	0.4

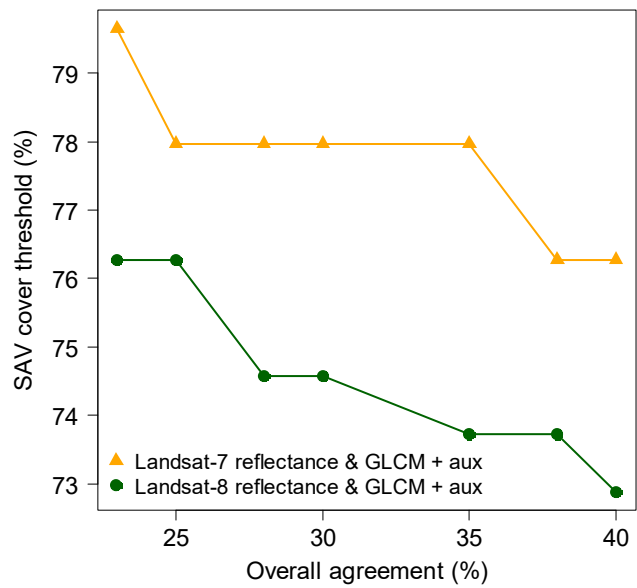


Figure A2. Plots of overall agreement/accuracies obtained from accuracy assessments of benthic habitat maps for the Bluefields Bay Special Fish Conservation Area (BBSFCA), Westmoreland, Jamaica, with (submerged aquatic vegetation present and absent and coral reef) created using different SAV percentage cover threshold increments (23%, 25% 28%, 30%, 35%, 38% and 40%). The maps were created using a (1) random forest (Rf) regression of acoustic SAV data points (dependent variable) and independent (auxiliary [aux]) data that included a bathymetric position index, band reflectance and Grey Level Co-Occurrence Matrix (GLCM) mean and variance data from either a Landsat-7 (2 bands) or Landsat 8 (2 bands) images.

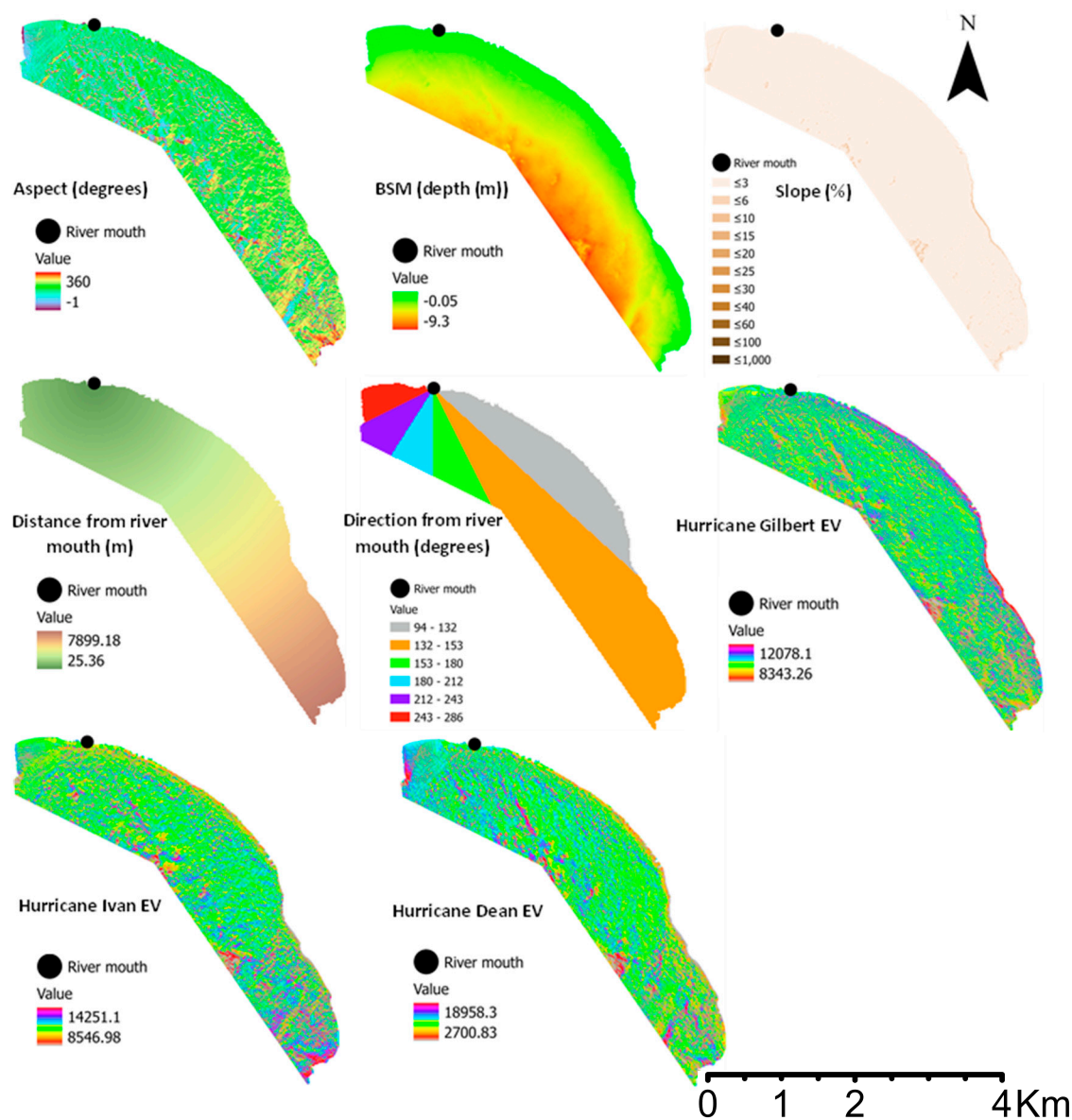


Figure A3. Maps of predictors used as predictors in the spatial Bayesian Integrated Nested Laplace Approximation (INLA) generalized linear mixed models to identify the best spatial pattern predictors of submerged aquatic vegetation (SAV) loss, gain and percentage cover change in the Bluefields Bay Special Fish Conservation Area (BBSFCA), Westmoreland, Jamaica. Value = min/max values. For aspect a value of - 1 = flat areas.

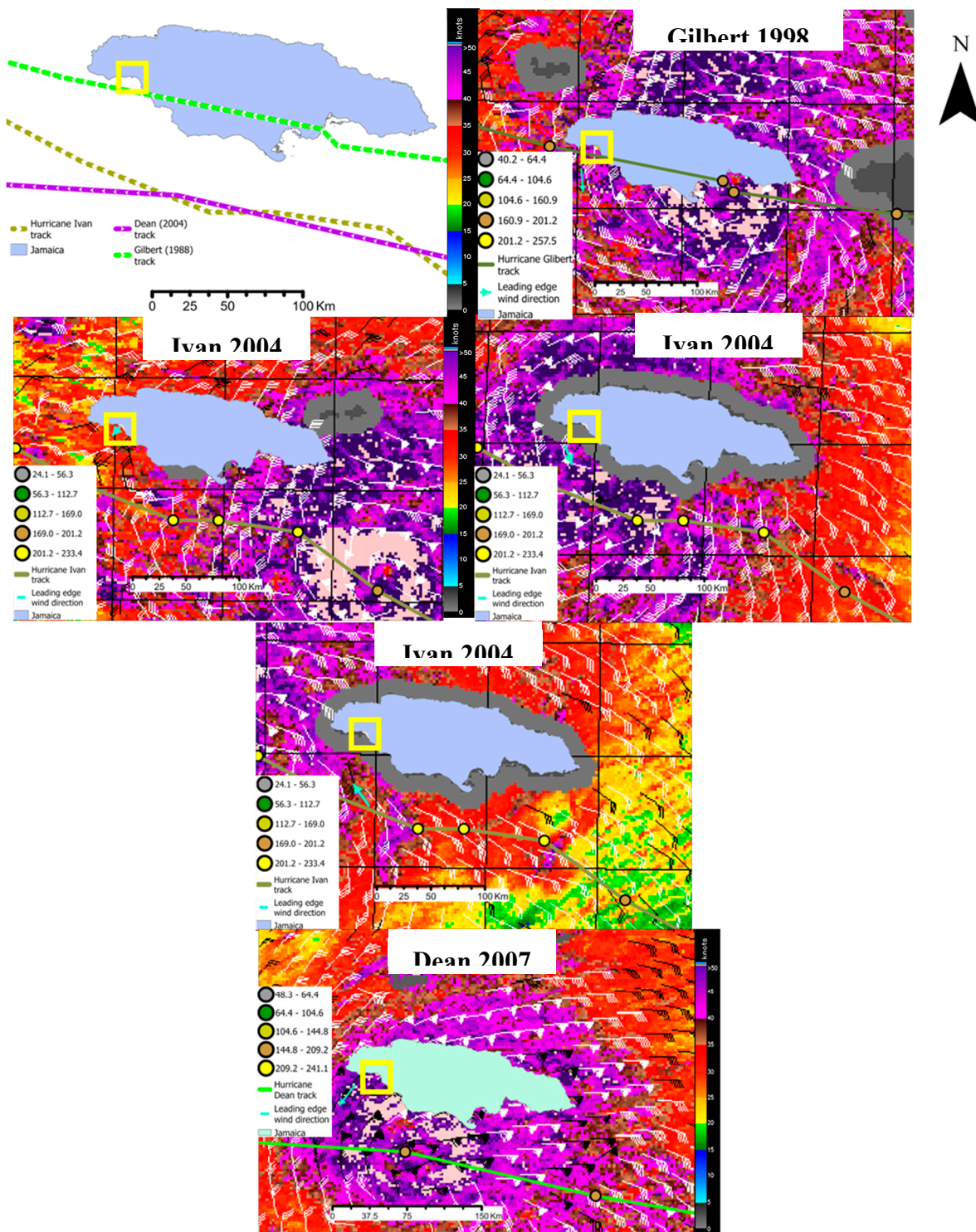


Figure A4. Tracks of (top right) the three hurricanes Gilbert – 1988, Ivan- 2004, and Dean-2007 that made landfall or passed by the island of Jamaica and had an effect on subaquatic vegetation (SAV) extent and percentage cover in the Bluefields Bay Special Fish Conservation Area (BBSFCA), Westmoreland, Jamaica (location highlighted by the yellow box (the hurricanes move from right to left). Also, a map of Jamaica overlaying processed ultra-high resolution images of hurricane winds created from QuikSCAT scatterometer satellite data (source <http://www.scp.byu.edu/data/Quikscat/HRStorms.html>), which contain information on wind speed (color coded) for the circular wind bands of hurricanes and information on wind direction (as wind flags). The leading edge wind direction is shown. The hurricane images include a proxy hurricane for Glibert centered on one of three track points used to calculate exposure vulnerability, and an image of Ivan as it passed by the island, that was dragged and centered on a track point some distance to

the east of the island and used to calculate EV for the hurricane before it passed by the island. Also, an image of Hurricane Dean over open water was dragged and centered on three track points close to Jamaica (one is shown).

References

1. Orth, R.J.; Carruthers, T.J.; Dennison, W.C.; Duarte, C.M.; Fourqurean, J.W.; Heck, K.L.; Hughes, A.R.; Kendrick, G.A.; Kenworthy, W.J.; Olyarnik, S. A global crisis for seagrass ecosystems. *Bioscience* **2006**, *56*, 987-996.
2. Unsworth, R.K.; McKenzie, L.J.; Collier, C.J.; Cullen-Unsworth, L.C.; Duarte, C.M.; Eklöf, J.S.; Jarvis, J.C.; Jones, B.L.; Nordlund, L.M. Global challenges for seagrass conservation. *Ambio* **2019**, *48*, 801-815.
3. Ralph, P.; Durako, M.J.; Enriquez, S.; Collier, C.; Doblin, M. Impact of light limitation on seagrasses. *Journal of experimental marine biology and ecology* **2007**, *350*, 176-193.
4. Horinouchi, M. Distribution patterns of benthic juvenile gobies in and around seagrass habitats: effectiveness of seagrass shelter against predators. *Estuarine, Coastal and Shelf Science* **2007**, *72*, 657-664.
5. Unsworth, R.K.; Nordlund, L.M.; Cullen-Unsworth, L.C. Seagrass meadows support global fisheries production. *Conservation Letters* **2019**, *12*, e12566.
6. Edgar, G.J.; Shaw, C. The production and trophic ecology of shallow-water fish assemblages in southern Australia I. Species richness, size-structure and production of fishes in Western Port, Victoria. *Journal of Experimental Marine Biology and Ecology* **1995**, *194*, 53-81.
7. Grech, A.; Chartrand-Miller, K.; Erftemeijer, P.; Fonseca, M.; McKenzie, L.; Rasheed, M.; Taylor, H.; Coles, R. A comparison of threats, vulnerabilities and management approaches in global seagrass bioregions. *Environmental Research Letters* **2012**, *7*, 024006.
8. Waycott, M.; Duarte, C.M.; Carruthers, T.J.; Orth, R.J.; Dennison, W.C.; Olyarnik, S.; Calladine, A.; Fourqurean, J.W.; Heck Jr, K.L.; Hughes, A.R. Accelerating loss of seagrasses across the globe threatens coastal ecosystems. *Proceedings of the national academy of sciences* **2009**, *106*, 12377-12381.
9. Lefcheck, J.S.; Orth, R.J.; Dennison, W.C.; Wilcox, D.J.; Murphy, R.R.; Keisman, J.; Gurbisz, C.; Hannam, M.; Landry, J.B.; Moore, K.A. Long-term nutrient reductions lead to the unprecedented recovery of a temperate coastal region. *Proceedings of the National Academy of Sciences* **2018**, *115*, 3658-3662.
10. Nordlund, L.M.; de la Torre-Castro, M.; Erlandsson, J.; Conand, C.; Muthiga, N.; Jiddawi, N.; Gullström, M. Intertidal zone management in the Western Indian Ocean: assessing current status and future possibilities using expert opinions. *Ambio* **2014**, *43*, 1006-1019.
11. Carlson, R.R.; Foo, S.A.; Asner, G.P. Land use impacts on coral reef health: A ridge-to-reef perspective. *Frontiers in Marine Science* **2019**, *6*, 562.
12. Fache, E.; Pauwels, S. The ridge-to-reef approach on Cicia Island, Fiji. *Ambio* **2022**, *51*, 2376-2388.
13. Brierley, A.S.; Kingsford, M.J. Impacts of climate change on marine organisms and ecosystems. *Current biology* **2009**, *19*, R602-R614.
14. Knutson, T.R.; McBride, J.L.; Chan, J.; Emanuel, K.; Holland, G.; Landsea, C.; Held, I.; Kossin, J.P.; Srivastava, A.; Sugi, M. Tropical cyclones and climate change. *Nature geoscience* **2010**, *3*, 157-163.
15. Chiang, F.; Mazdiyasni, O.; AghaKouchak, A. Evidence of anthropogenic impacts on global drought frequency, duration, and intensity. *Nature communications* **2021**, *12*, 2754.
16. Thornton, P.K.; Ericksen, P.J.; Herrero, M.; Challinor, A.J. Climate variability and vulnerability to climate change: a review. *Global change biology* **2014**, *20*, 3313-3328.
17. Kim, K.; Choi, J.-K.; Ryu, J.-H.; Jeong, H.J.; Lee, K.; Park, M.G.; Kim, K.Y. Observation of typhoon-induced seagrass die-off using remote sensing. *Estuarine, Coastal and Shelf Science* **2015**, *154*, 111-121.
18. Côté-Laurin, M.-C.; Benbow, S.; Erzini, K. The short-term impacts of a cyclone on seagrass communities in Southwest Madagascar. *Continental Shelf Research* **2017**, *138*, 132-141.
19. Hall, M.O.; Furman, B.T.; Merello, M.; Durako, M.J. Recurrence of *Thalassia testudinum* seagrass die-off in Florida Bay, USA: initial observations. *Marine Ecology Progress Series* **2016**, *560*, 243-249.
20. León-Pérez, M.C.; Armstrong, R.A.; Hernández, W.J.; Aguilar-Perera, A.; Thompson-Grim, J. Seagrass cover expansion off Caja de Muertos Island, Puerto Rico, as determined by long-term analysis of historical aerial and satellite images (1950–2014). *Ecological Indicators* **2020**, *117*, 106561.
21. Congdon, V.M.; Hall, M.O.; Furman, B.T.; Campbell, J.E.; Durako, M.J.; Goodin, K.L.; Dunton, K.H. Common ecological indicators identify changes in seagrass condition following disturbances in the Gulf of Mexico. *Ecological Indicators* **2023**, *156*, 111090.

22. Chollett, I.; Bone, D.; Pérez, D. Effects of heavy rainfall on *Thalassia testudinum* beds. *Aquatic Botany* **2007**, *87*, 189-195.
23. Evans, S.M.; Griffin, K.J.; Blick, R.A.; Poore, A.G.; Vergés, A. Seagrass on the brink: Decline of threatened seagrass *Posidonia australis* continues following protection. *Plos one* **2018**, *13*, e0190370.
24. Mancini, G.; Mastrantonio, G.; Pollice, A.; Lasinio, G.J.; Belluscio, A.; Casoli, E.; Pace, D.S.; Ardizzone, G.; Ventura, D. Detecting trends in seagrass cover through aerial imagery interpretation: Historical dynamics of a *Posidonia oceanica* meadow subjected to anthropogenic disturbance. *Ecological Indicators* **2023**, *150*, 110209.
25. Lecours, V. On the use of maps and models in conservation and resource management (warning: results may vary). *Frontiers in Marine Science* **2017**, *4*, 288.
26. Barrell, J.; Grant, J. Detecting hot and cold spots in a seagrass landscape using local indicators of spatial association. *Landscape ecology* **2013**, *28*, 2005-2018.
27. Phinn, S.; Roelfsema, C.; Dekker, A.; Brando, V.; Anstee, J. Mapping seagrass species, cover and biomass in shallow waters: An assessment of satellite multi-spectral and airborne hyper-spectral imaging systems in Moreton Bay (Australia). *Remote sensing of Environment* **2008**, *112*, 3413-3425.
28. Baumstark, R.; Dixon, B.; Carlson, P.; Palandro, D.; Kolasa, K. Alternative spatially enhanced integrative techniques for mapping seagrass in Florida's marine ecosystem. *International Journal of Remote Sensing* **2013**, *34*, 1248-1264.
29. Vahtmäe, E.; Paavel, B.; Kutser, T. How much benthic information can be retrieved with hyperspectral sensor from the optically complex coastal waters? *Journal of Applied Remote Sensing* **2020**, *14*, 016504-016504.
30. McIntyre, K.; McLaren, K.; Prospere, K. Mapping shallow nearshore benthic features in a Caribbean marine-protected area: assessing the efficacy of using different data types (hydroacoustic versus satellite images) and classification techniques. *International Journal of Remote Sensing* **2018**, *39*, 1117-1150.
31. McLaren, K.; McIntyre, K.; Prospere, K. Using the random forest algorithm to integrate hydroacoustic data with satellite images to improve the mapping of shallow nearshore benthic features in a marine protected area in Jamaica. *GIScience & Remote Sensing* **2019**, *56*, 1065-1092.
32. Newman, M.E.; McLaren, K.P.; Wilson, B.S. Long-term socio-economic and spatial pattern drivers of land cover change in a Caribbean tropical moist forest, the Cockpit Country, Jamaica. *Agriculture, Ecosystems & Environment* **2014**, *186*, 185-200.
33. Lambin, E.F.; Geist, H.J.; Lepers, E. Dynamics of land-use and land-cover change in tropical regions. *Annual review of environment and resources* **2003**, *28*, 205-241.
34. Kamwi, J.M.; Cho, M.A.; Kaetsch, C.; Manda, S.O.; Graz, F.P.; Chirwa, P.W. Assessing the spatial drivers of land use and land cover change in the protected and communal areas of the Zambezi Region, Namibia. *Land* **2018**, *7*, 131.
35. McIntyre, K. Benthic mapping of the Bluefields Bay fish sanctuary, Jamaica. *LUMA-GIS Thesis* **2015**.
36. McLaren, K.; Luke, D.; Tanner, E.; Bellingham, P.J.; Healey, J.R. Reconstructing the effects of hurricanes over 155 years on the structure and diversity of trees in two tropical montane rainforests in Jamaica. *Agricultural and Forest Meteorology* **2019**, *276*, 107621.
37. Majka, D.; Jenness, J.; Beier, P. CorridorDesigner: ArcGIS tools for designing and evaluating corridors. Available at <http://corridordesign.org/>. **2007**.
38. R Core Team, R.; Team, R.C. R: a language and environment for statistical computing. R Foundation for Statistical Computing. <http://www.R-project.org/>. **2022**.
39. R Core Team, R.; Team, R.C. R: a language and environment for statistical computing. R Foundation for Statistical Computing. <http://www.R-project.org/>. **2023**.
40. Zvoleff, A. Package 'glcm'. Calculate Textures from Grey-Level Co-Occurrence Matrices (GLCMs). Available online: <https://cran.r-project.org/web/packages/glcm/index.html> (accessed on 25 October 2022) **2020**.
41. Liaw, A.; Wiener, M. Classification and regression by randomForest. *R news* **2002**, *2*, 18-22.
42. Bakar, K.S.; Sahu, S.K. spTimer: Spatio-temporal Bayesian modeling using R. *Journal of Statistical Software* **2015**, *63*, 1-32.
43. Aho, K. asbio: A Collection of Statistical Tools for Biologists_. R package version 1.9-6. . <<https://CRAN.R-project.org/package=asbio>> **2023**.
44. Wood, S.N. Fast stable restricted maximum likelihood and marginal likelihood estimation of semiparametric generalized linear models. *Journal of the Royal Statistical Society Series B: Statistical Methodology* **2011**, *73*, 3-36.

45. Wood, S.N. *Generalized additive models: an introduction with R*; CRC press: 2017.
46. Wood, S.N. Stable and efficient multiple smoothing parameter estimation for generalized additive models. *Journal of the American Statistical Association* **2004**, *99*, 673-686.
47. Wood, S.N.; Pya, N.; Säfken, B. Smoothing parameter and model selection for general smooth models. *Journal of the American Statistical Association* **2016**, *111*, 1548-1563.
48. Zuur, A.F.; Ieno, E.N.; Walker, N.J.; Saveliev, A.A.; Smith, G.M. *Mixed effects models and extensions in ecology with R*; Springer: 2009; Volume 574.
49. Hyndman, R.; Athanasopoulos, G.; Bergmeir, C.; Caceres, G.; Chhay, L.; O'Hara-Wild, M.; Petropoulos, F.; Razbash, S.; Wang, E.; Yasmien, F. forecast: Forecasting functions for time series and linear models. R package version 8.21.1. <<https://pkg.robjhyndman.com/forecast/>>. **2023**.
50. Hyndman, R.J.; Khandakar, Y. Automatic time series forecasting: the forecast package for R. *Journal of statistical software* **2008**, *27*, 1-22.
51. Bates, D.; Mächler, M.; Bolker, B.; Walker, S. Fitting linear mixed-effects models using lme4. *arXiv preprint arXiv:1406.5823* **2014**.
52. Luke, D.; McLaren, K.; Wilson, B. Modeling hurricane exposure in a Caribbean lower montane tropical wet forest: The effects of frequent, intermediate disturbances and topography on forest structural dynamics and composition. *Ecosystems* **2016**, *19*, 1178-1195.
53. Knapp, K.R.; Kruk, M.C.; Levinson, D.H.; Diamond, H.J.; Neumann, C.J. The international best track archive for climate stewardship (IBTrACS) unifying tropical cyclone data. *Bulletin of the American Meteorological Society* **2010**, *91*, 363-376.
54. Knapp, K.R., H. J. Diamond, J. P. Kossin, M. C. Kruk, C. J. Schreck. International Best Track Archive for Climate Stewardship (IBTrACS) Project, Version 4. North Atlantic. NOAA National Centers for Environmental Information. **2018**, doi:10.25921/82ty-9e16.
55. Mikita, T.; Klimánek, M. Topographic exposure and its practical applications. *Journal of Landscape Ecology* **2010**, *3*, 42-51.
56. Batke, S.P.; Jocque, M.; Kelly, D.L. Modelling hurricane exposure and wind speed on a mesoclimate scale: a case study from Cusuco NP, Honduras. *PloS one* **2014**, *9*, e91306.
57. Lindgren, F.; Rue, H. Bayesian spatial modelling with R-INLA. *Journal of statistical software* **2015**, *63*.
58. Lindgren, F.; Rue, H.; Lindström, J. An explicit link between Gaussian fields and Gaussian Markov random fields: the stochastic partial differential equation approach. *Journal of the Royal Statistical Society Series B: Statistical Methodology* **2011**, *73*, 423-498.
59. Rue, H.; Martino, S.; Chopin, N. Approximate Bayesian inference for latent Gaussian models by using integrated nested Laplace approximations. *Journal of the Royal Statistical Society Series B: Statistical Methodology* **2009**, *71*, 319-392.
60. Rue, H.; Riebler, A.; Sørbye, S.H.; Illian, J.B.; Simpson, D.P.; Lindgren, F.K. Bayesian computing with INLA: a review. *Annual Review of Statistics and Its Application* **2017**, *4*, 395-421.
61. Martins, T.G.; Simpson, D.; Lindgren, F.; Rue, H. Bayesian computing with INLA: new features. *Computational Statistics & Data Analysis* **2013**, *67*, 68-83.
62. Rue, H.; Martino, S. Approximate Bayesian inference for hierarchical Gaussian Markov random field models. *Journal of statistical planning and inference* **2007**, *137*, 3177-3192.
63. Cosandey-Godin, A.; Krainski, E.T.; Worm, B.; Flemming, J.M. Applying Bayesian spatiotemporal models to fisheries bycatch in the Canadian Arctic. *Canadian Journal of Fisheries and Aquatic Sciences* **2015**, *72*, 186-197.
64. Fuglstad, G.-A.; Simpson, D.; Lindgren, F.; Rue, H. Constructing priors that penalize the complexity of Gaussian random fields. *Journal of the American Statistical Association* **2019**, *114*, 445-452.
65. Illian, J.B.; Sørbye, S.H.; Rue, H.; Hendrichsen, D.K. Using INLA to fit a complex point process model with temporally varying effects-a case study. *Journal of Environmental Statistics* **2012**, *3*.
66. Spiegelhalter, D.J.; Best, N.G.; Carlin, B.P.; Van Der Linde, A. Bayesian measures of model complexity and fit. *Journal of the Royal Statistical Society Series B: Statistical Methodology* **2002**, *64*, 583-639.
67. Zheng, B. Summarizing the goodness of fit of generalized linear models for longitudinal data. *Statistics in medicine* **2000**, *19*, 1265-1275.
68. Robin, X.; Turck, N.; Hainard, A.; Tiberti, N.; Lisacek, F.; Sanchez, J.-C.; Müller, M. pROC: an open-source package for R and S+ to analyze and compare ROC curves. *BMC bioinformatics* **2011**, *12*, 1-8.

69. Sørbye, S.H. Tutorial: scaling IGMRF-models in R-INLA. *University of Tromsø, Tromsø, Department of Mathematics and Statistics* **2013**.
70. Rodemann, J.R.; James, W.R.; Santos, R.O.; Furman, B.T.; Fratto, Z.W.; Bautista, V.; Lara Hernandez, J.; Viadero, N.M.; Linenfelser, J.O.; Lacy, L.A. Impact of extreme disturbances on suspended sediment in western Florida Bay: implications for seagrass resilience. *Frontiers in Marine Science* **2021**, *8*, 633240.
71. McKenna, S.; Jarvis, J.; Sankey, T.; Reason, C.; Coles, R.; Rasheed, M. Declines of seagrasses in a tropical harbour, North Queensland, Australia, are not the result of a single event. *Journal of biosciences* **2015**, *40*, 389-398.
72. Shelton, A.O.; Francis, T.B.; Feist, B.E.; Williams, G.D.; Lindquist, A.; Levin, P.S. Forty years of seagrass population stability and resilience in an urbanizing estuary. *Journal of Ecology* **2017**, *105*, 458-470.
73. Ahmad-Kamil, E.; Ramli, R.; Jaaman, S.; Bali, J.; Al-Obaidi, J. The effects of water parameters on monthly seagrass percentage cover in Lawas, East Malaysia. *The Scientific World Journal* **2013**, 2013.
74. Marbà, N.; Duarte, C.M. Interannual changes in seagrass (*Posidonia oceanica*) growth and environmental change in the Spanish Mediterranean littoral zone. *Limnology and oceanography* **1997**, *42*, 800-810.
75. Campbell, S.J.; McKenzie, L.J. Flood related loss and recovery of intertidal seagrass meadows in southern Queensland, Australia. *Estuarine, Coastal and Shelf Science* **2004**, *60*, 477-490.
76. de Fouw, J.; Govers, L.L.; van de Koppel, J.; van Belzen, J.; Dorigo, W.; Cheikh, M.A.S.; Christianen, M.J.; van der Reijden, K.J.; van der Geest, M.; Piersma, T. Drought, mutualism breakdown, and landscape-scale degradation of seagrass beds. *Current Biology* **2016**, *26*, 1051-1056.
77. Khogkhao, C.; Hayashizaki, K.-i.; Tuntiprapas, P.; Prathep, A. Changes in seagrass communities along the runoff gradient of the Trang river, Thailand. *ScienceAsia* **2017**, *43*, 339-346.
78. Shivers, S.D.; Golladay, S.W.; Waters, M.N.; Wilde, S.B.; Ashford, P.D.; Covich, A.P. Changes in submerged aquatic vegetation (SAV) coverage caused by extended drought and flood pulses. *Lake and Reservoir Management* **2018**, *34*, 199-210.
79. Agawin, N.S.; Duarte, C.M.; Fortes, M.D. Nutrient limitation of Philippine seagrasses (Cape Bolinao, NW Philippines): in situ experimental evidence. *Marine Ecology Progress Series* **1996**, *138*, 233-243.
80. Terrados, J.; Agawin, N.S.; Duarte, C.M.; Fortes, M.D.; Kamp-Nielsen, L.; Borum, J. Nutrient limitation of the tropical seagrass *Enhalus acoroides* (L.) Royle in Cape Bolinao, NW Philippines. *Aquatic Botany* **1999**, *65*, 123-139.
81. Vieira, V.M.; Lobo-Arteaga, J.; Santos, R.; Leitão-Silva, D.; Veronez, A.; Neves, J.M.; Nogueira, M.; Creed, J.C.; Bertelli, C.M.; Samper-Villarreal, J. Seagrasses benefit from mild anthropogenic nutrient additions. *Frontiers in Marine Science* **2022**, *9*, 960249.
82. Camacho, R.; Houk, P. Decoupling seasonal and temporal dynamics of macroalgal canopy cover in seagrass beds. *Journal of Experimental Marine Biology and Ecology* **2020**, *525*, 151310.
83. Hernández-Delgado, E.A.; Toledo-Hernández, C.; Ruiz-Díaz, C.; Gómez-Andújar, N.; Medina-Muñiz, J.; Canals-Silander, M.; Suleimán-Ramos, S. Hurricane impacts and the resilience of the invasive sea vine, *Halophila stipulacea*: A case study from Puerto Rico. *Estuaries and Coasts* **2020**, *43*, 1263-1283.
84. Oprandi, A.; Mucerino, L.; De Leo, F.; Bianchi, C.; Morri, C.; Azzola, A.; Benelli, F.; Besio, G.; Ferrari, M.; Montefalcone, M. Effects of a severe storm on seagrass meadows. *Science of the Total Environment* **2020**, *748*, 141373.
85. Marco-Méndez, C.; Marbà, N.; Amores, Á.; Romero, J.; Minguito-Frutos, M.; García, M.; Pagès, J.F.; Prado, P.; Boada, J.; Sánchez-Lizaso, J.L. Evaluating the extent and impact of the extreme Storm Gloria on *Posidonia oceanica* seagrass meadows. *Science of The Total Environment* **2024**, *908*, 168404.
86. Correia, K.M.; Smee, D.L. A meta-analysis of tropical cyclone effects on seagrass meadows. *Wetlands* **2022**, *42*, 108.
87. Enríquez, S.; Olivé, I.; Cayabyab, N.; Hedley, J.D. Structural complexity governs seagrass acclimatization to depth with relevant consequences for meadow production, macrophyte diversity and habitat carbon storage capacity. *Scientific Reports* **2019**, *9*, 14657.
88. Krause-Jensen, D.; Quaresma, A.L.; Cunha, A.H.; Greve, T. How are seagrass distribution and abundance monitored. *European seagrasses: An introduction to monitoring and management* **2004**, 45-53.

Disclaimer/Publisher's Note: The statements, opinions and data contained in all publications are solely those of the individual author(s) and contributor(s) and not of MDPI and/or the editor(s). MDPI and/or the editor(s) disclaim responsibility for any injury to people or property resulting from any ideas, methods, instructions or products referred to in the content.